NAVAL POSTGRADUATE SCHOOL

MONTEREY, CALIFORNIA

THESIS

MECHANICAL BEHAVIOR OF COLD SPRAYED CU-NI COATING

by

Adrian Chua

September 2021

Thesis Advisor:	Andy Nieto
Co-Advisor:	Troy Ansell
Second Reader:	Chanman Park

THIS PAGE INTENTIONALLY LEFT BLANK

REPORT DOCUMENTATION PAGE			*Form Approved OMB No. 0704-0188*

1. AGENCY USE ONLY *(Leave blank)*	**2. REPORT DATE** September 2021	**3. REPORT TYPE AND DATES COVERED** Master's thesis

4. TITLE AND SUBTITLE MECHANICAL BEHAVIOR OF COLD SPRAYED CU-NI COATING	**5. FUNDING NUMBERS** Naval Research Program Project; (IREF) ID: NPS-21-N
6. AUTHOR(S) Adrian Chua	
7. PERFORMING ORGANIZATION NAME(S) AND ADDRESS(ES) Naval Postgraduate School Monterey, CA 93943-5000	**8. PERFORMING ORGANIZATION REPORT NUMBER**
9. SPONSORING / MONITORING AGENCY NAME(S) AND ADDRESS(ES) Naval Research Program CA 93943	**10. SPONSORING / MONITORING AGENCY REPORT NUMBER**

11. SUPPLEMENTARY NOTES The views expressed in this thesis are those of the author and do not reflect the official policy or position of the Department of Defense or the U.S. Government.

12a. DISTRIBUTION / AVAILABILITY STATEMENT Approved for public release. Distribution is unlimited.	**12b. DISTRIBUTION CODE** A

13. ABSTRACT (maximum 200 words)

Cold spray is a developing additive-manufacturing technology well suited as a preventive and corrective measure for metallic materials. The key challenge lies in formulating the optimal multifaceted spray parameters to achieve a functional coating on a substrate. Copper-nickel (Cu-Ni) alloy is particularly suited for study, due to its feasibility as both coating and repair material to be deposited onto a substrate through cold spray technology and its well-established characteristics for corrosion protection and mechanical strength. This thesis studied the change in mechanical behavior due to annealing of cold-sprayed Cu-Ni coating. In order to do so, the subject Cu-Ni powder's behavior and coating quality were characterized through the variation of certain spray parameters and examined by the mechanical behavior of multiple passes of Cu-Ni coatings through tensile testing, adhesion testing and nanoindentation testing. The as-sprayed coating exhibited brittleness and had weak mechanical interlocking adhesion with the substrate. Annealing mitigates and delays the mechanical deficiencies associated with porosity in the coating, which showed signs of the stronger metallurgical bonding with the substrate. Annealed cold spray coating itself can bear significant load and strengthen the substrate. Thus, cold spray coating with appropriate post-processing treatment can potentially reinforce and even repair the component to achieve robust mechanical behavior.

14. SUBJECT TERMS copper-nickel, Cu-Ni, cold spray, tensile, adhesion, nanoindentation, heat treatment, Young's modulus, hardness, plasticity	**15. NUMBER OF PAGES** 95
	16. PRICE CODE

17. SECURITY CLASSIFICATION OF REPORT Unclassified	**18. SECURITY CLASSIFICATION OF THIS PAGE** Unclassified	**19. SECURITY CLASSIFICATION OF ABSTRACT** Unclassified	**20. LIMITATION OF ABSTRACT** UU

NSN 7540-01-280-5500

Standard Form 298 (Rev. 2-89)
Prescribed by ANSI Std. 239-18

THIS PAGE INTENTIONALLY LEFT BLANK

Approved for public release. Distribution is unlimited.

MECHANICAL BEHAVIOR OF COLD SPRAYED CU-NI COATING

Adrian Chua
Military Expert 5, Republic of Singapore Air Force
BME, Nanyang Technological University, 2009

Submitted in partial fulfillment of the
requirements for the degree of

MASTER OF SCIENCE IN MECHANICAL ENGINEERING

from the

NAVAL POSTGRADUATE SCHOOL
September 2021

Approved by: Andy Nieto
Advisor

Troy Ansell
Co-Advisor

Chanman Park
Second Reader

Garth V. Hobson
Chair, Department of Mechanical and Aerospace Engineering

THIS PAGE INTENTIONALLY LEFT BLANK

ABSTRACT

Cold spray is a developing additive-manufacturing technology well suited as a preventive and corrective measure for metallic materials. The key challenge lies in formulating the optimal multifaceted spray parameters to achieve a functional coating on a substrate. Copper-nickel (Cu-Ni) alloy is particularly suited for study, due to its feasibility as both coating and repair material to be deposited onto a substrate through cold spray technology and its well-established characteristics for corrosion protection and mechanical strength. This thesis studied the change in mechanical behavior due to annealing of cold-sprayed Cu-Ni coating. In order to do so, the subject Cu-Ni powder's behavior and coating quality were characterized through the variation of certain spray parameters and examined by the mechanical behavior of multiple passes of Cu-Ni coatings through tensile testing, adhesion testing and nanoindentation testing. The as-sprayed coating exhibited brittleness and had weak mechanical interlocking adhesion with the substrate. Annealing mitigates and delays the mechanical deficiencies associated with porosity in the coating, which showed signs of the stronger metallurgical bonding with the substrate. Annealed cold spray coating itself can bear significant load and strengthen the substrate. Thus, cold spray coating with appropriate post-processing treatment can potentially reinforce and even repair the component to achieve robust mechanical behavior.

THIS PAGE INTENTIONALLY LEFT BLANK

TABLE OF CONTENTS

LIST OF FIGURES

THIS PAGE INTENTIONALLY LEFT BLANK

LIST OF TABLES

THIS PAGE INTENTIONALLY LEFT BLANK

LIST OF ACRONYMS AND ABBREVIATIONS

Al	aluminum
ASTM	American Society for Testing and Materials
CP	commercially pure
Cu	copper
DE	deposition efficiency
He	helium
N_2	nitrogen
Ni	nickel
SEM	scanning electron microscopy
UTS	ultimate tensile strength
YS	yield strength

THIS PAGE INTENTIONALLY LEFT BLANK

ACKNOWLEDGMENTS

The author would like to express his gratitude to Professor Andy Nieto, Professor Troy Ansell, and Professor Chanman Park for their guidance and patience during the endeavor of this thesis. The author would also like to extend his appreciation to Mr. John Mobley for his effort and time to prepare and machine the specimens.

THIS PAGE INTENTIONALLY LEFT BLANK

I. INTRODUCTION

A. THESIS MOTIVATION

Corrosion is a perennial issue applicable to all industries due to the magnitude of oxidation promoters in the environment. For naval operations, the sea exacerbates its extensiveness due to the presence of salt and microbes [1], [2] in addition to the corrosive gases and chemicals used onboard the vessels. Corrosion is being comprehensively addressed with both preventive and corrective measures. Cold spray technology is a viable technology to be adopted for both protective and corrective measures through the deposition of metallic coating particles. Cold spray technology thus has extended use in additive manufacturing. Copper-Nickel (Cu-Ni) alloy is particularly suited for study due to (1) its feasibility as both coating and repair material to be deposited onto a substrate through cold spray technology [3], and (2) its well-established characteristics for corrosion protection and mechanical properties' reinforcement [4]. The Cu-Ni alloy forms a binary isomorphous system with single phase field as shown in Figure 1 because of the complete solubility of Cu and Ni to form solid solution [5]. The presence of Ni in Cu results in the lattice strain interaction between the dislocations and strained Ni atoms that is known as solid-solution strengthening in which solute atoms restrict the dislocations' movement [5]. The increase in tensile strength and yield strength corresponds to an increase in Ni content shown in Figure 2.

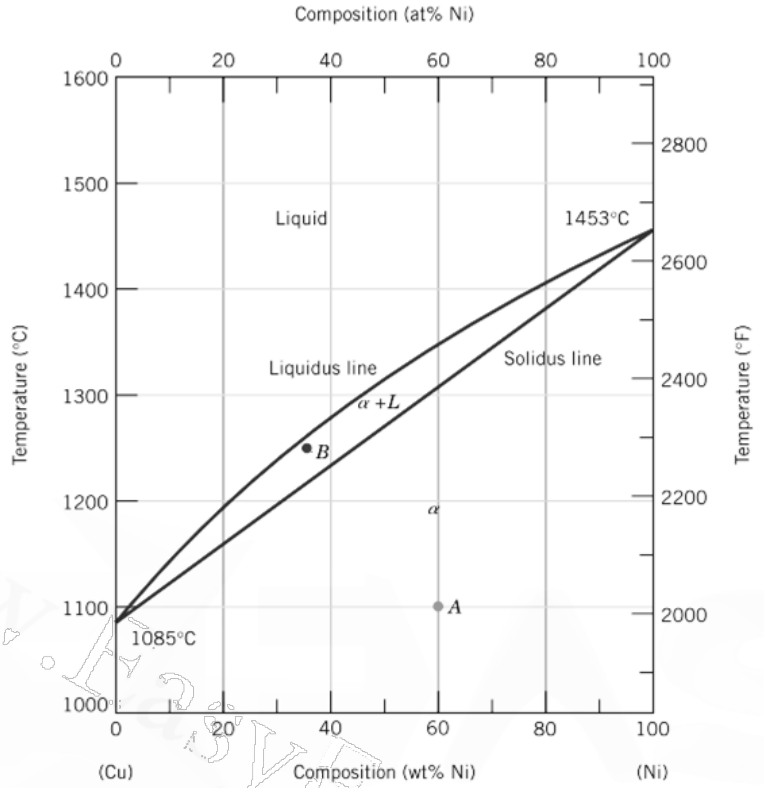

Figure 1. Cu-Ni Phase Diagram. Source: [5].

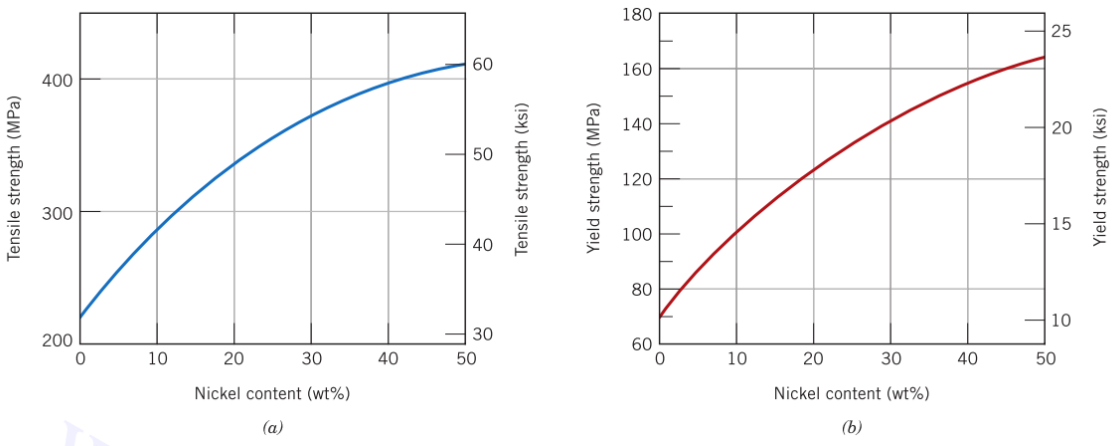

Figure 2. Variation with Ni Content of (a) Tensile Strength, and (b) Yield Strength for Cu-Ni Alloys. Source: [5].

B. STATE-OF-THE-ART REVIEW OF COLD SPRAY TECHNOLOGY

1. Genesis of Cold Spray

Prior to the accidental discovery of cold spray technology by the former Soviet Union in the 1980s, thermal spray was the predominant coating technology to apply coatings over materials. Thermal spray utilizes both thermal energy (through the high processing temperature to melt the coating material) and kinetic energy (through the spraying force of melted material over the target substrate) [6]. The drawback of thermal spray arises from the high processing temperature required, which can result in the following internal defects in the coating:

- decarburization where carbon is lost in the surface-adjacent zone of a carbide-containing material,
- dissolution where a solute dissolves in a solvent to form a solution, and
- delamination where coating and substrate splits apart into layers due to thermal mismatch.

In contrast, cold spray eliminates the need to melt the coating material and utilizes kinetic energy gained through the ejection of supersonic coating particles onto the target substrate to result in the adhesion. Figure 3 illustrates the difference in energy sources for both coating technologies.

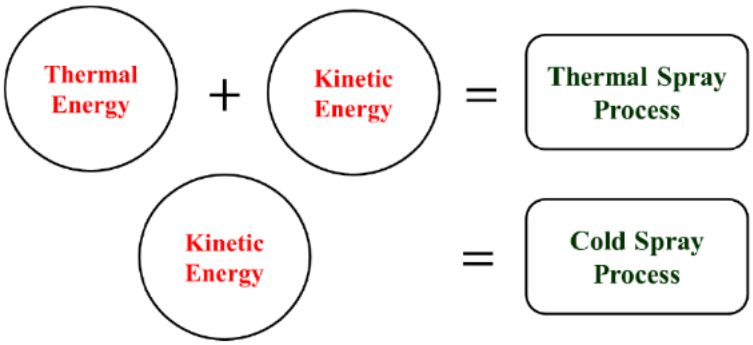

Figure 3. Difference in Energy Sources for Both Coating Technologies. Source: [6].

2. Working Principle of Cold Spray

The working principle is to accelerate the coating particles through a de Laval nozzle (also known as a converging-diverging nozzle) where the particles are accelerated out from the nozzle at supersonic velocity to impact onto the substrate and prior sprayed particles. There are two main types of adhesion that occur. The first adhesion type is metallurgical bonding which results from local adiabatic shear instabilities. This phenomenon arises from the extensive plastic deformation and thermal softening of both the substrate and coating particles during repeated impacts. The extensively flattened coating particles formed outward jet at its rim to clear oxide film present on the coating particles and substate, which allows direct adhesion contact [7]. Thus, metallurgical bonding can happen at the interfaces of (1) particle-substrate, and (2) particle-particle. The second adhesion type is mechanical interlocking, in which the coating particle is physically entrapped within the substrate surface due to the physical impact and adiabatic shear flow. However, there is a third adhesion phenomenon known as intertwining with features of particle elongation and fracture observed at the coating-substrate interface in limited cases when hard coating particles (such as Ni) were deposited onto soft substrate (such as aluminum Al) [8]. The ultrafine grains noted inside a deposited and deformed particle implied that the impact of a subsequent particles could cause a local high-strain-rate shear band necessary for the deformation. The fracture behavior was dominated by sliding mode, tearing mode, and a hybrid of both modes. Figure 4 illustrates the three adhesion types described.

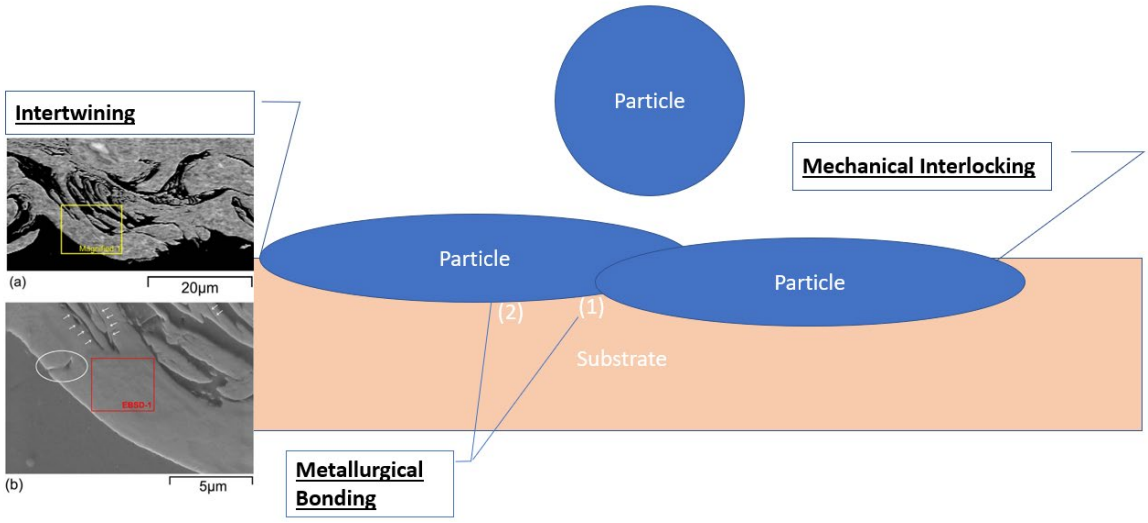

Figure 4. Three Adhesion Types Are Illustrated: (a) Mechanical Interlocking where the Substrate Physically Entraps the Particles, (b) Metallurgical Bonding where the Local Adiabatic Shear Instabilities at (1) Particle-Particle Interface, and (2) Particle-Substrate Interface, Arise from the Extensive Plastic Deformation and Thermal Softening due to the Impact, and (c) Intertwining (shown with SEM Images at (a) Low Magnification, and (b) High Magnification) where the Particles and Substrate Mutually Intertwine through Particle Elongation and Fracture. SEM Source: [8].

3. Factors for Performance of Cold Spray Coating

The control of the working parameters is pivotal for deposition efficiency (DE) and coating quality of each spray. DE is defined as the percentage of spent powder that consolidates into the final component [9] shown in Equation 1. The desired mechanical properties and fatigue performance of the sprayed coating are resultant from the balanced permutations amongst four variables groups summarized in Figure 5 [8]–[36].

$$\text{Deposition Efficiency, DE (\%)} = \left(\frac{\Delta(\text{Weight of Powder})}{\Delta(\text{Weight of Specimen})} \right) \times 100 \qquad (1)$$

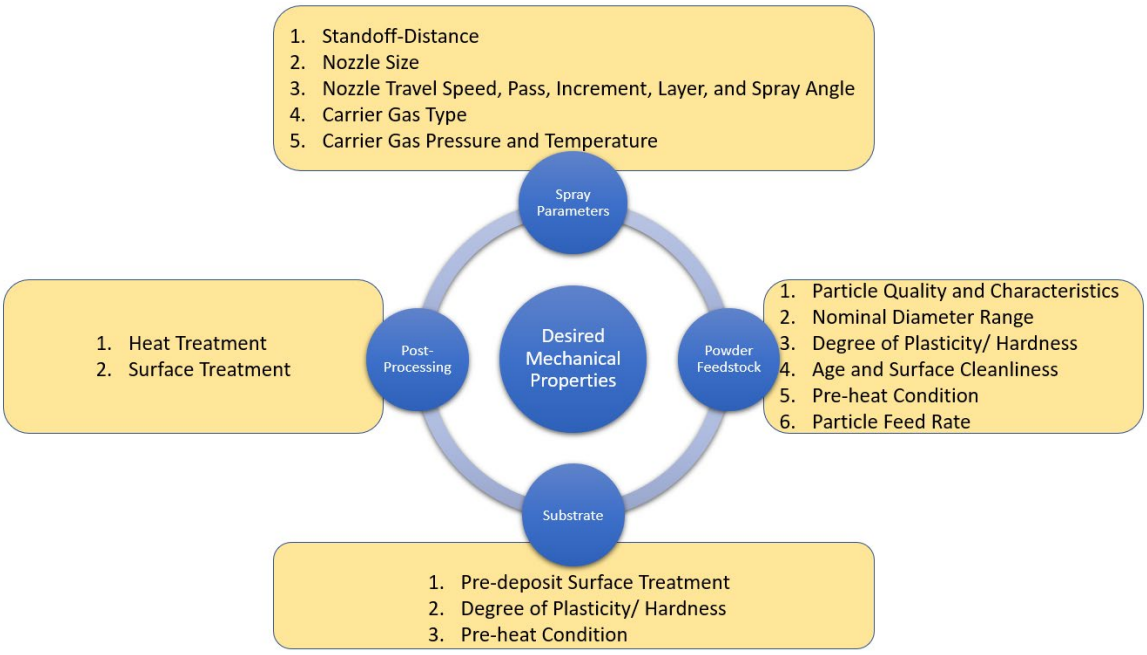

Figure 5. Overview of Working Parameters for Cold Spray.

- Coating Powder. The mechanical properties of the coating powder influence its performance from its ejection from the nozzle to their impact onto the substrate. To name a few, the physical dimensions of the coating particles is consequential to the critical velocity required to result in the metallurgical bonding and mechanical interlocking, as well as the degree of porosity in the coating. On a separate note, as mentioned by Nastic et al. [9], the coating particles' state changes with time and whether they are recycled. In addition, there are studies that investigated the consequence on the DE with regard to the pre-heating of the coating particles in order to soften them prior to their ejection from the nozzle. The results by Yang et al. [10] documented that the fatigue lifetime of the Q355B steel specimens coated with the smaller A5052 powder (average particle size was 14.71 μm) is 62.61% higher than those specimens coated with the larger Al powder (average particle size was 22.25 μm), which is then relatively 36.49% longer than that of the unsprayed specimens. In contrast, Cavaliere et al. [11] concluded that larger particles dimensions of IN625 Ni-based powder (particle size distribution of 45+15 μm) showed lower porosity in coatings with higher

energy density leading to strain hardening. Both characteristics were beneficial for fatigue performance and resulted in transgranular fracture with local plastic deformition observed in those zones where particle cohesion was stronger. The contrasting conclusions suggest there are multi-faceted factors for fatigue performance of different materials beyond the simplistic consideration of particle size alone. The addition of ceramic particles, such as Al_2O_3 into the powder was shown by Xiong et al. [12] to improve the bonding strength and coating density through its hammering effect. The stronger coating vis-à-vis the substrate and the better bonding with the substrate resulted in improved yield and tensile strength of the coated substrate.

- Substrate. Like the coating particles, the surface condition and state of the substrate are consequential to the adhesion of the coating particles at the crucial interface. Plastic strain energy from the particles' collision upon the substrate is preserved when the pre-heated substrate softens adequately to reduce the rate of strain hardening [6]. Smoother Ti64 substrate surface due to grinding and milling was found to have better fatigue performance for the Ti64 coated sample [13]. This is because of the stronger coating-substrate adhesion. The resultant lower porosity at the interface could attribute less crack initiation from the interface into the coating. This finding is contrary to the findings by Ziemian et al. [14] that surface roughness at macro-level need to be high enough for better particle-substrate adhesion interface while reduce the oxide layer found on metal alloy such as Al oxide on Al. Ziemian et al. [14] also showed that the substrates that were glass-bead grit blasted had better fatigue performance improvement when compared to shot-peening. Ghelichi et al. [15] explained that the compressive residual stresses in the substrate can be attributed to the grit blasting treatment and cold spray's peening effect. It also suggested that the gas temperature can anneal the substrate to result in limited offload of residual stresses induced by grit blasting and cold spray. This illustrated the complex considerations for the inter-relationship of each process parameters.

- Spray Parameters. The working parameters for the spray nozzle, such as nozzle standoff distance and carrier gas (such as nitrogen N_2 or helium He), will influence the resultant kinetic energy of the ejected coating particles which in turn translates to the resultant DE and mechanical properties of the coating [16]. The choice of carrier gas to propel the coating particles affects (a) the annealing effect that the coating particles can induce onto the substrate through the carried kinetic energy, (b) the degree that the coating particles can be pre-heated, (c) the application of varying gas pressures, (d) the intentional/unintentional raising of substrate's temperature, and (e) the reduction possibility for oxidation [17], [18]. The choice of carrier gas was also reportedly to influence the coating's microstructure and the diffusion mechanism within the particle-particle interfaces when annealed [19]. However, there is subjectivity in the suitability of carrier gas with specific material. For instance, Barnes et al. [20] found with surprise that cold spray Commercially Pure (CP) Al coatings using N_2 carrier gas had higher residual compressive stress and better adhesion performance under bend test than those sprayed with He gas. However, the coatings produced using He gas displayed lower mean porosity values than those coated using N_2 due to the higher particle velocity achievable with He. Thus, Barnes et al. highlighted that more studies are required to explain their findings. The conclusion regarding lower porosity when using He gas was independently confirmed in [21] and is the current conventional understanding to achieve dense coating.

- Post-Processing. Post-processing can alter the performance of the coating and substrate. Post-spray shot-peening can reduce coating surface's roughness by flattening the coating with the peening shots [22]. This reduction in the number of stress risers on the coating will improve its fatigue performance. However, the fatigue benefit to induce residual compressive stress onto the substrate is less significant as compared to performing SP prior to cold spray. In addition, post-spray shot-peening may cause spalling of the coating. The post-spray heat treatment of cold sprayed coating can improve the ductility and other mechanical properties by strengthening the inter-particle bonding with recrystallization [23].

This can mitigate the degree of surface damage induced by post-spray shot-peening as well as to improve the coating's ductility. Barnes et al. [20] found that T76 heat treatment mitigated the reduction effect in the Ultimate Tensile Strength (UTS), Yield Strength (YS) and elongation percentage of the cold sprayed Al 7075 alloy with CP Al as compared to the uncoated substrate. Paul et al. [24] explained that the elastic modulus of the coatings with hierarchical particle layout can be increased via splat sintering enable by the heat treatment. Pertaining to Cu and Ni, some of the heat treatment-related researches suggested that recrystallization of Cu-Ni alloys occurs in the temperature range of 527 ^{o}C to 1,100 ^{o}C [19], [24]–[26]. Yamamoto et al. [25] found that the thickness of the diffusion-induced recrystallization region has near-square root correlation to the annealing time regardless of the composition of Ni when the Cu-Ni to Ni couple were annealed at 600 ^{o}C. The micro-hardness data seen in [26] shows the softening of the various Cu-Ni alloys after being annealed beyond 550 ^{o}C for 1 hour. Specific to cold sprayed coating, Stoltenhoff et al. [19] reported that the microstructures of the coatings sprayed showed recrystallized grains and improvement in conductivity from 63% to 92% of the International Anneal Copper Standard (γ = 57.14 m/(Ω cm)) for oxygen-free bulk copper at room temperature (20 ^{o}C) after being annealed at 600 ^{o}C for 1 hour. The hardness reduction with increasing annealing temperature was also reported to plateau around 300 ^{o}C. Despite the mentioned benefits from heat treatment, more material-specific research is needed to ascertain the beneficial extent. Kumar et al. [27] noted and summarized a few supporting literatures that metallic bonding at the inter-splat boundaries can be induced when heat treatment is done at 0.4 to 0.5 of the coating particle's melting temperature. Koivuluoto et al. [23] found that particle boundaries of the dense Ni-30%Cu coatings were not made increasingly visible with increasing heat treatment temperature from 400 to 600, 800 and 1,000 ^{o}C annealed for 5 hours in an argon environment. However, it was noted that the degree of etching decreased with the increased heat treatment, in which the

authors alluded to recrystallization that could had made the coating denser with lesser inter-particle voids.

4. Literatures Related to Cold Spray of Cu and Ni

There are some general understandings of Cu-based and Ni-based cold sprayed coatings, as well as general coating properties that can be gleaned from these studies.

- Metallurgical. Multiple studies [28], [29], [30] found that regardless of the particle size, the DE for N_2 gas with preheated powders is higher than the sole use of He gas. Insufficiently energized particles can rebound from the impact surface when the particle velocity is less than the critical velocity to result in low DE (< 50%), while overly-energized particles can erode the coating after reaching the maximum DE (100%). By increasing powder preheat temperature, the DE and coating quality can improve with (a) reduced crack formation and porosity, (b) increased microhardness, and (c) better adhesive strength. The increased hardness of the coating is due to the particles' strain hardening upon impact and the tamping effect of both high-velocity impacted and rebounded particles that densified the coating [29]. Nautiyal et al. [31] noted low inter-splat crack density can result in high modulus reduction in the coating. In addition, the particle splat and substrate deformed as a system rather than individually when plasticity is high. However, microhardness was also found to decrease with an increase in particle sizes. The study [29] concluded that the smallest particle size (26 to 44 μm) with a high 90% DE had the optimal mechanical performance vis-a-vis the bond strength and microhardness that are adequate for conventional engineering usages, in contrast to the larger particle sizes (37 to 74 μm). To recap, Cavaliere et al. [11] found that Ni-based Diamalloy 1005 with larger particles dimensions (45+15 μm) showed lower porosity levels in coating. Transgranular fracture with localized plastic deformation was observed in those zones where particles cohesion was stronger. Zou et al. [32] highlighted that the observation of ultrafine grains in the Ni-coating's particle-particle boundaries, which is evident of recrystallization. The authors quoted two possible mechanisms for dynamic

recrystallization which are rotational and migrational types. These types differ in their misorientation movement from the original grains vis-à-vis the recrystallized region. He attributed the observed ultrafine grains to the dynamic recrystallization produced by lattice and subgrain rotations. Yin et al. [7] noted that mechanical interlocking is easier to achieve with high temperature substrate due to its' decreased YS and being thermally softened. Furthermore, the high temperature substrate eased the atomic mixture between the substrate and the particles at their interface to result in the stronger metallurgical bonding. These factors led to coating mass increase and better coating–substrate bonding strength with high-temperature substrate. Pertaining to Cu coating, Nastic et al. [9] noted that the non-spherical Cu powders achieved higher DE than spherical Cu powders under the same spray condition. While non-spherical particles could theoretically be faster than spherical particles, this does not always improve the deposition. Li et al. [33] observed cracks and interlocking at the interfaces of Cu particles. This suggested that the main bonding mechanism between the Cu particles to be mechanical interlocking. Cu coating with varying degree of deformation will have heterogeneous mechanical property that correlates to the amount of dislocations accumulated near the grain boundaries.

- Corrosion. Reference [3] was a Ni-specific research regarding the structural and corrosion properties of the following powders that were cold sprayed with high pressure: (a) Ni, (b) Ni-Cu, and (c) Ni-Cu with ceramic addition (Al_2O_3). The study noted that Ni coatings with post-sprayed heat treatment retained the ability to form a stable layer over a wide potential range. In addition, the annealed Ni coatings showed lower corrosion current density and higher polarization resistance than those of as-sprayed Ni coatings. It was also noted that the Al_2O_3 improves the densification and corrosion resistance of the Ni-Cu coatings. Higher preheat spraying temperature and post-spray heat treatment improved the corrosion resistance of the coatings through their densification by recrystallization and void reduction. In corrosive environments, the corrosion resistance of Ni-Cu with Al_2O_3 coating was better than the pure Ni-Cu coating due to its lower

corrosion current density and higher polarization resistance vis-à-vis the bulk materials. Separate studies by Xie et al. [18] and Wei et al. [34] found that the Ni coating prepared via in-situ shot-peening assisted cold spraying showed similar corrosion resistance vis-a-vis the electroless Ni-based coating. The shot-peened Ni coating surface did not have apparent appearance change and had minute weight loss to corrosion with no spall-off coating vis-à-vis the as-sprayed coating.

- Mechanical Behavior. Porosity affects the coatings' mechanical behavior. IN625 Ni-based coating cold sprayed at high pressure of 5 MPa and 1,000 °C was found to possesses lower porosity below 1%, higher plasticity index of 0.037 and lower corrosion current, when compared to coatings sprayed at 4 MPa and 800 °C [35]. The less porous coating resulted in pronounced ductile fracture and positively inhibited crack propagation. This finding was independently confirmed by Xie et al. [18] and Wei et al. [34], which found that the pores and microcracks became smaller with the particles preheated at higher temperature. The preheating process also relived the work hardening effect resulted from deposition, thus reduced the coating's microhardness when the porosity was reduced. The optimal particle preheating temperature using air as the working gas for highest adhesion strength was approximately 200 °C. On a separate note, increasing heat treatment temperature can reduce the hardness of the coating as heat treatment mend the inter-splat cracks through solid-state diffusion [36]. On separate study regarding Cu, the hardness of the highly deformed zone on the cold sprayed Cu coating had irregular standard deviations due to the extensive plastic deformation [33]. This factor also caused the Young's modulus of small deformed zones of the Cu coating to be higher than that of the large deformed zones. Both the tamping effect of particle onto preceding particle simulated by Yin et al. [37] and the shear deformation could had reduced the Cu coating's hardness, which led to the reduced ability to resist the crack initiation and propagation.

- Fatigue. Pristine cold sprayed coating aid the fatigue performance of the substrate. Amongst the limited fatigue-related studies on cold sprayed Cu or Ni coating,

Silvello et al. [35] noted that less porous IN625 Ni-based coating led to stable and slow crack propagation through the coating's thickness. The ductility and hardness in the coating resulted in observable striations which indicates the coating's fatigue performance. In the broad-scoped review by Cavaliere and Silvello [17], it underlined that those coatings observed with "low porosity, high adhesion strength and high superficial compressive residual stresses" demonstrated better fatigue properties. The dynamic recrystallisation due to the severe plastic deformation of the particles impacting the surface induced compressive residual stress in the nanocrystalline microstructure at the coating-substrate interface that acted as crack initiation delay. It also noted that low porosity in coating is also achievable with low pressure cold spray through adjusting other process parameters. Bagherifard and Guagliano [38] further explained that another key variable to the cold sprayed samples' fatigue performance is the extent of compressive residual stresses induced by (1) the shot peening effect by the particles and (2) the buildup of coating layers. It was also cautioned that strong adhesion achieved by using weaker coating powder than that of the substrate can degrade the substrate's fatigue performance instead as an enhancement, as cracks initiated in the weaker coating can propagate into the metallurgically adhered substrate.

C. THESIS OBJECTIVES

With reference to the motivations and current understanding of cold sprayed Cu and Ni related properties mentioned in the prior sections, this thesis aims to delve beyond the scope of those studies by addressing the following aspects of the subject Cu-Ni powder:

- Characterize the powder's behavior and resultant coating quality influenced by carrier gas pressure, carrier gas temperature, feed rate, travel speed and number of passes.

- Characterize the mechanical behavior of Cu-Ni coating, through examine the metallurgical properties of the Cu-Ni powder, tensile and adhesion strengths, Young's modulus and hardness of the Cu-Ni coatings,
- Study the change in mechanical behavior of substrate due to annealing.

II. EXPERIMENTAL PROCEDURES

A. MATERIALS

1. Coating Particles

Atomized Cu-Ni alloy CU-116 (Cu-38Ni) from Praxair Surface Technologies Inc. was used. It comprises Ni with 38 wt% with the approximate powder diameter of 45 μm and melting temperature in range of 1,083 to 1,455 ºC [39, 40]. Reference to Figure 1, the liquidus and solidus temperatures are approximately 1,270 ºC and 1,230 ºC, respectively. The powder is stored in a furnace to dehumidify it prior to spraying. Figure 6 shows the scanning electron microscopy (SEM) images of the powder at various magnifications.

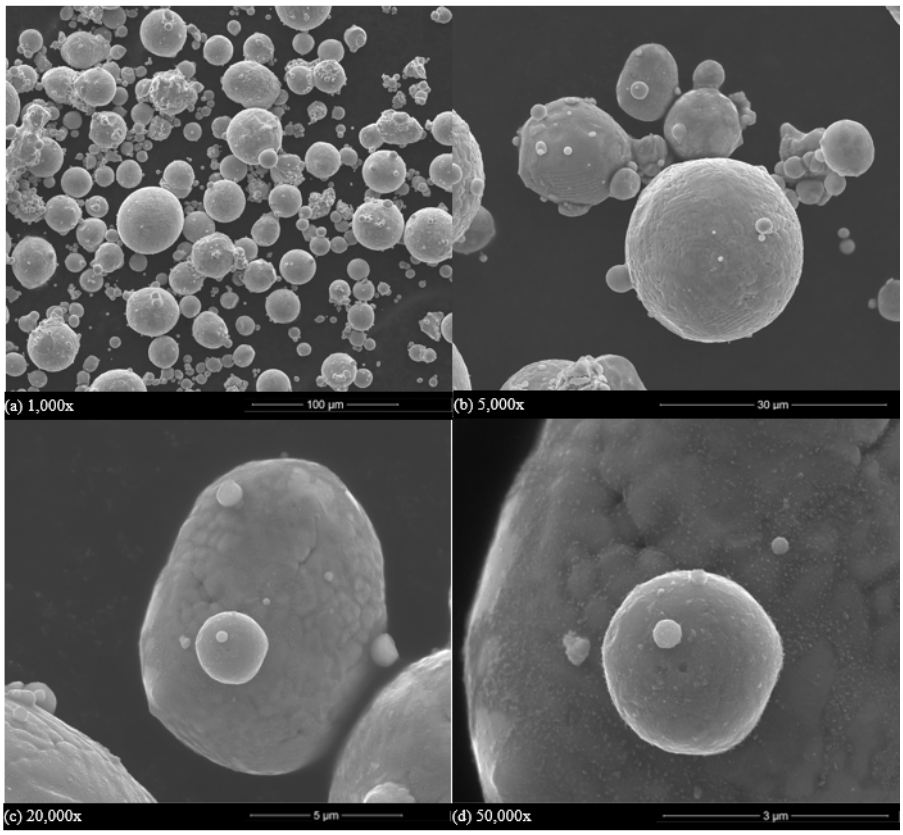

Figure 6. SEM Images of Cu-38Ni Powder That Showed the Relative Spherical Shape of the Particles at Magnifications of (a) 1,00x, (b) 5,000x, (c) 20,000x, and (d) 50,000x.

2. Substrate

C70600 Cu90-Ni10 (Cu-10Ni) flat sheets with thickness of 6.35mm (0.25”) produced by KME Germany Mansfeld GmbH & Co. KG were procured. Based on open sources [41], [42], Cu-10Ni has Poisson’s ratio of 0.34 and melting temperature in range of 1,099 ºC to 1149 ºC. Referencing to Figure 1, the liquidus and solidus temperatures are approximately 1,150 ºC and 1,125 ºC, respectively. Beads of 100–170 grit were used to grit-blasted the plates, while the mirror-polished plates were polished from 80-grit to 1,200-grit as shown in Figure 7.

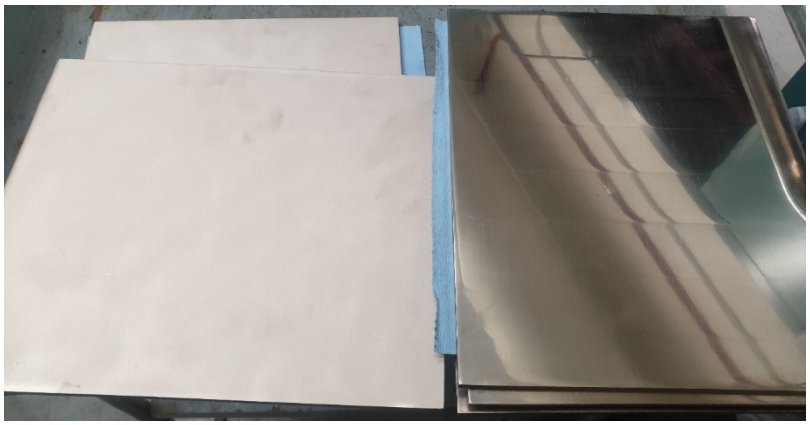

Figure 7. Grit-Blasted and Mirror-Polished Cu-Ni Plates.

3. Specimen Groups

The specimens were grouped into four categories: (a) mirror-polished specimens (substrate), (b) annealed mirror-polished specimens (annealed substrate), (c) as-sprayed grit-blasted specimens (coated), and (d) annealed cold-sprayed grit-blasted specimens (annealed coated). The rationale for mirror-polished specimens is to establish a pristine reference, while the grit-blasted specimens would promote good coating-substrate adhesion. Subsize tensile specimens per American Society for Testing and Materials (ASTM) E8/E8M - 09 standard with the dimensions shown in Figure 8 were computer numerical control cut to minimize stress risers in the specimens.

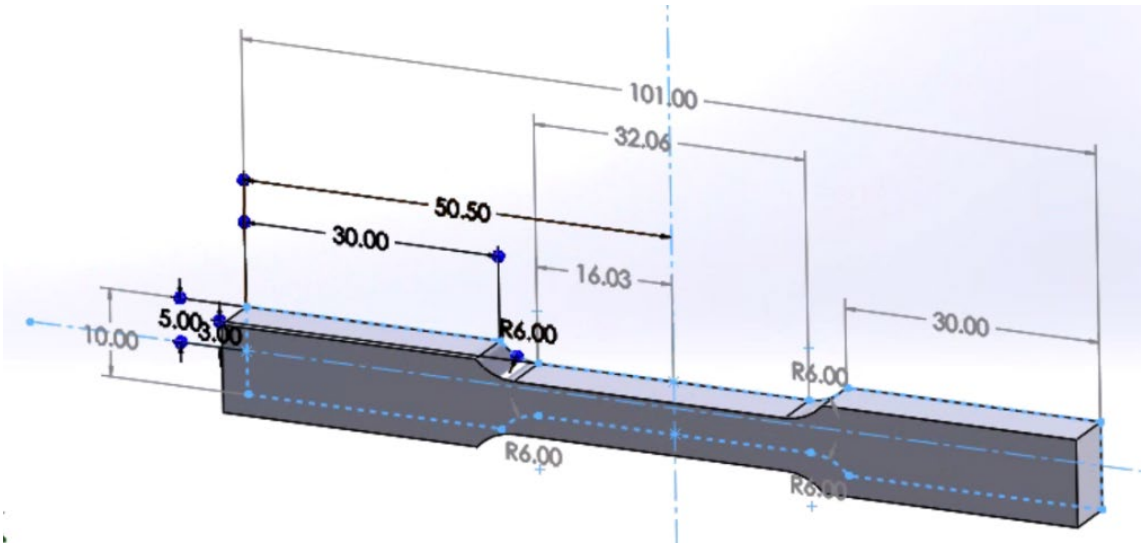

Figure 8. Dimensions of Subsized Specimens per ASTM E8/E8M Standard in Millimeters.

B. PROCESSING

1. Cold Spray

SST PX Manual-Automatic Split Cabinet with Wet Dust Collection System and SST X-Feeder shown in Figure 9 were used to deposit the Cu-38Ni coating particles. For SST PX Manual-Automatic Split Cabinet, the SST Automatic P gun attached to a Cartesian XY robot was used to minimize coating variation [43]. SST X-Feeder supply non-pressurized and vibration-assisted powder feeding to the positively pressurized control cabinet with pressure monitoring to keep electronics free of metal particles. SST X-Feeder can support feed rate up to 120 g/min with powder capacity of 1000 ml per canister [44]. Cu-38Ni was sprayed onto the grit-blasted plate with the parameters shown in Table 1.

Figure 9. SST PX Manual-Automatic Split Cabinet (Left) and SST X-Feeder (Right).

Table 1. Spray Parameters.

Parameters	Setting
Nozzle Diameter Size	6.35 mm
Nozzle Standoff Distance	12.70 mm
Nozzle Travel Speed	30 mm/s
Spray Angle	90º
Number of Passes	2
Carrier Gas	Nitrogen
Carrier Gas Pressure	1.379 MPa
Carrier Gas Temperature	500 ºC
Powder Feed Rate	15% (18 g/min)

2. Heat Treatment

MTI Corporation's OTF-1200X shown in Figure 10 was used for the heat treatment of the cold-sprayed specimens. OTF-1200X has continuous working temperature range from 100 ºC to 1,100 ºC and achieve fast heating up to 1,200 ºC at maximum heating rate of 20 ºC per minute over its two heating zones [45]. The specimens were heated to 650 ºC with ramp time of 90 minutes and annealed for 60 minutes before cooled in OTF-1200X for 3.5 hours under 0.03 MPa argon environment. The anneal temperature is defined based on the consideration of the materials' melting temperatures and the literatures referenced.

Figure 10. MTI Corporation's OTF-1200X.

C. MECHANICAL TESTING

1. Adhesion Test

Two adhesives were used for this thesis. Their key specifications relevant to this thesis are shown in Table 2.

Table 2. Adhesives' Key Specifications.

	Masterbond EP15ND-2 [46]	**J-B Weld Steel Reinforced Epoxy 8265S [47]**
Tensile Strength	82.74 MPa	34.61 MPa
Cure Temperature	148.89 ºC to 176.67 ºC	Room temperature (20 ºC)
Cure Time	60 minutes to 90 minutes	15 hours to 24 hours

Cole-Parmer's Conventional Laboratory Oven 05015-60 shown in Figure 11 was used to cure the Masterbond EP15ND-2 Adhesive on specimens. 05015-60 has working temperature range from 50 ºC to 200 ºC controlled by a bimetallic thermostat and requires a glass mercury thermometer to display the temperature. Although 05015-60 is unable to maintain a constant temperature environment, it was operated at temperature range of 150 ºC to 169 ºC which is within Masterbond EP15ND-2 Adhesive's recommended curing temperature range.

Figure 11. Cole-Parmer's Conventional Laboratory Oven 05015-60 (Right).

ELCOMETER 510 Model T shown in Figure 12 was used for the adhesion test. With an automatic hydraulic pump, smooth load application up to 100 MPa can be adjustably exerted at pull rates of 0.1-1.4 MPa/s with accuracy of ±1% of the full scale [48]. Dollies of 10 mm diameter were adhered to the test specimens and pulled till failure at 552 kPa/sec to observe for adhesive or coating failure. The stress values were read off from ELCOMETER 510 Model T.

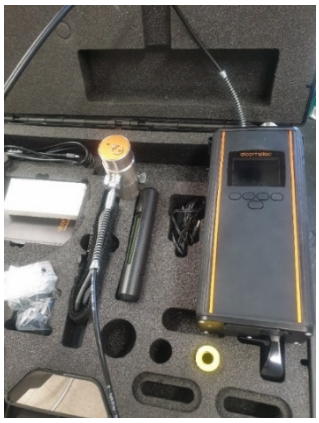

Figure 12. ELCOMETER 510 Model T.

2. Tensile Test

INSTRON 5982 Universal Testing Instrument shown in Figure 13 was used for the tensile test. It has force capacity up to 100 kn and load measurement accuracy to +/-

0.5% of reading down to 1/1000 of load cell capacity [49]. It is also capable of synchronized data acquisition rates up to 2,500 points per second. The specimens were subjected to 2 mm/min. Based on the dimensions referencing (ASTM) E8/E8M - 09 standard, the original specimen length L_o is 3.206 x 10^{-2} m, and original area A is 3.81 x 10^{-5} m^2. The area considering the average coating thickness is 3.81 x 10-^{5} m^2. INSTRON 5982 provides both the load value F and the change in displacement ΔL, which allows the derivation of maximum length L_{max}. With the load-displacement response data extracted, the strain, stress and elongation-to-rupture for each specimen are calculated using equation (2) to (4), respectively.

Figure 13. INSTRON 5982 Universal Testing Instrument.

$$\text{Strain, } \varepsilon \text{ (mm/mm)} = \frac{\Delta L \text{ (mm)}}{L_o \text{(mm)}} \tag{2}$$

$$\text{Stress, } \sigma \text{ (MPa)} = \frac{F \text{ (N)}}{A \text{ (mm}^2\text{)}} \tag{3}$$

$$\text{Elongation-to-Rupture, } \delta \text{ (\%)} = \left(\frac{L_{Max} \text{ (mm)}}{L_0 \text{ (mm)}} \right) \times 100 \tag{4}$$

3. Nanoindentation Test

AGILENT's Nanoindenter G200 shown in Figure 14 equipped with nanomechanical actuating transducer allows continuous stiffness measurement with accurate displacement resolution up to 0.01 nm and load resolution up to 50 nN, due to the stability of permanent magnetic field and lateral stiffness from the two leaf springs [50]. The maximum allowable load is 500 mN or 50 gF. The specimens were indented with 5 gF per load over 10 seconds and held for 3 seconds before being off-loaded over 10 seconds. Each specimen region was indented at 30 spots to gather statistical representation while account for possible measurement failure. Cu-10Ni's Poisson's ratio of 0.34 is assumed for both as-sprayed and annealed coatings for the program to derive the Young's modulus.

Plasticity refers to the plastic deformation sustained by the test region after the indentation and is estimated vide Equation (5). Reading off from the plots, $L_{Plastic}$ is the last displacement value upon the full off-load of the indenter, and L_{max} is the maximum displacement achieved. Higher plasticity corresponds to higher ductility in the material as it gets elongated and manifested as dimples on fracture surface. Contact stiffness is estimated by Nanoindenter G200 using the maximum amount of force offloaded over one unit of recovered displacement as shown in Equation (6). Nanoindenter G200 then based on the estimated contact stiffness to derive the test material's Young's modulus vide Equation (7) and Equation (8) referenced from [50], where ν is test material's Poisson's ratio, ν_i is the diamond indenter's Poisson's ratio and E_i is Young's modulus of the diamond indenter.

Figure 14. AGILENT Nanoindenter G200.

$$\text{Plasticity (\%)} = \left(\frac{\mathrm{L_{Plastic}}}{\mathrm{L_{Max}}}\right)\times 100 \tag{5}$$

$$\text{Contact Stiffness, S (N/m)} = \left(\frac{d\mathrm{F}}{d\mathrm{L}}\right)_{\mathrm{L}_{Max}} \tag{6}$$

$$\text{Reduced Modulus, } \mathrm{E}_r \text{ (GPa)} = \left(\frac{\sqrt{\pi}}{2}\right)\left(\frac{\mathrm{S(N/m)}}{\sqrt{\mathrm{A}}\,\mathrm{(m)}}\right) \tag{7}$$

$$\text{Young's Modulus, E (GPa)} = \left(1-\nu^2\right)\left(\frac{1}{E_r}-\frac{1-\nu_i^{\,2}}{E_i}\right)^{-1} \tag{8}$$

D. CHARACTERIZATION

1. Specimen Preparation

All the specimens used in this thesis were grinded with grinding papers from 320-grit, to 600-grit, 800-grit and finally 1,200-grit. The specimens were then polished with 3-μm and 1- μm diamond suspension to reduce much of the scratch marks.

Etchant is an acid solution used to attack the grain boundaries to make them prominent. For this thesis, the etchant composition of 1 part nitric acid, 1 part acetic acid, and 2 parts acetone is used [51]. The coated and annealed coated specimens were etched for 30 seconds, rinsed with distilled water and cleaned with methanol.

2. Metallurgical Inspection

FEI's Inspect F50 Scanning Electron Microscope shown in Figure 15 was used for high magnification metallurgical examination of the specimens. It is equipped with a high resolution Schottky field emission electron optics with accelerating voltages from 200 V up to 30 kV [52]. Coupled with the Everhart-Thornley secondary electron detector, Inspect F50 can achieved magnification between 14 to 10^6 times. The specimens were inspected using 20 kV and magnifications up to 10,000 times.

Figure 15. FEI Inspect F50 SEM.

Nikon Model Epiphot 200 Microscope paired with Nikon Digital Sight DS-2Mv shown in Figure 16 were used for coating-substrate interface inspection at lower magnification. The Nikon Model Epiphot 200 Microscope is equipped with objective lenses at magnification from 2.5 times to 100 times. It is able to observe specimen under both brightfield and darkfield with polarization [53]. Nikon Digital Sight DS-2Mv allows the digital image to be captured.

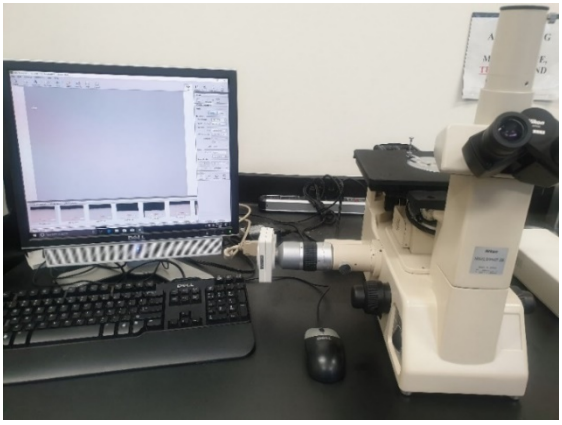

Figure 16. Nikon Model Epiphot 200 Microscope and Nikon Digital Sight DS-2Mv.

III. RESULTS AND DISCUSSIONS

A. RESULTS

1. Trials to Define Spray Parameters

Trials were conducted on an as-received plate to understand the coating characteristics under the different permutations of spray parameters. One of the requirements from the topic sponsor Naval Sea Systems Command was for the coating thickness to be at least 10% to 15% of the substrate thickness. Hence, the target coating thickness is between 0.635 mm (10%) to 0.953 mm (15%). Five variables were chosen to aid in the characterization with the intent for thick coating: (a) Carrier Gas Temperature, (b) Carrier Gas Pressure, (c) Feed Rate, (d) Travel Speed, and (e) Number of Passes.

a. Coating Thickness

The trial started with the variations of the carrier gas temperatures (300 ^{o}C, 400 ^{o}C and 500 ^{o}C) and pressures (0.69 MPa, 1.03 MPa and 1.38 MPa). The thickest coating was achieved with 500 ^{o}C and 1.38 MPa. More trials proceeded with the variation of the feed rate, travel speed and number of passes to achieve the thickest coating. Table 3 summarized the coating thicknesses measured from the digital images of those trial specimens' cross-sectional view. The sets of parameters that achieved 9% and above of the target coating thickness are highlighted in the red box. The big standard deviation is attributed to the unevenness of the coatings.

Table 3. Trials' Coating Thickness Measurements.

Carrier Gas Temp. (^{o}C)	500									
Carrier Gas Pressure (MPa)	1.24		1.38							
No. of Passes	4	2	4	2	4	2	2	2	2	2
Feed Rate (%)	10	20	4	4	6	10	15	15	20	20
Travel Speed (mm/s)	40	30	30	40	30	40	30	20	30	40
Average (µm)	313.80	436.27	372.79	144.12	502.52	248.22	570.31	622.96	652.91	455.04
Std Dev (µm)	157.97	15.61	6.11	14.43	10.00	39.09	22.46	21.79	17.97	15.41

(1) Matched Correlation of Coating Thickness with Feed Rate and Travel Speed

Table 4 shows the summary of thickness-per-pass for all the trials conducted with carrier gas at 500 ºC and 1.379 MPa. The observed trend matches the current understanding of thicker coating with lower travel speed and higher feed rate. The data from the chart shown for travel speed at 30 mm/s in Figure 17 suggests that the optimal feed rate to be 15% before the plateau effect begins. Figure 18 shows the similar trend for travel speed at 40 mm/s. However, the plateau effect was not observed as trial for 15% feed rate was not conducted.

Table 4. Summary of Thickness-Per-Pass Measurements.

Travel Speed / Feed rate	**20 mm/s**	**30 mm/s**	**40 mm/s**
4%	N.A.	0.0933 mm/pass	0.072 mm/pass
6%	N.A.	0.126 mm/pass	N.A.
10%	N.A.	N.A.	0.124 mm/pass
15%	0.312 mm/pass	0.287 mm/pass	N.A.
20%	N.A.	0.321 mm/pass	0.228 mm/pass

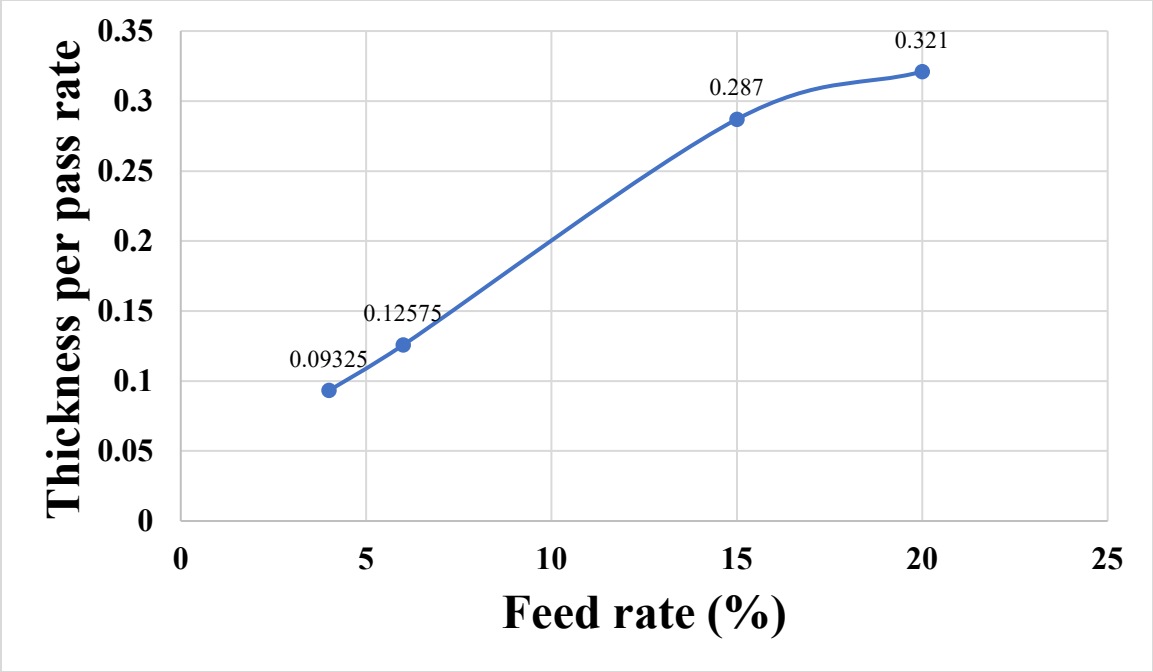

Figure 17. Feed Rate to Thickness-per-pass Rate Correlation at 30 mm/s.

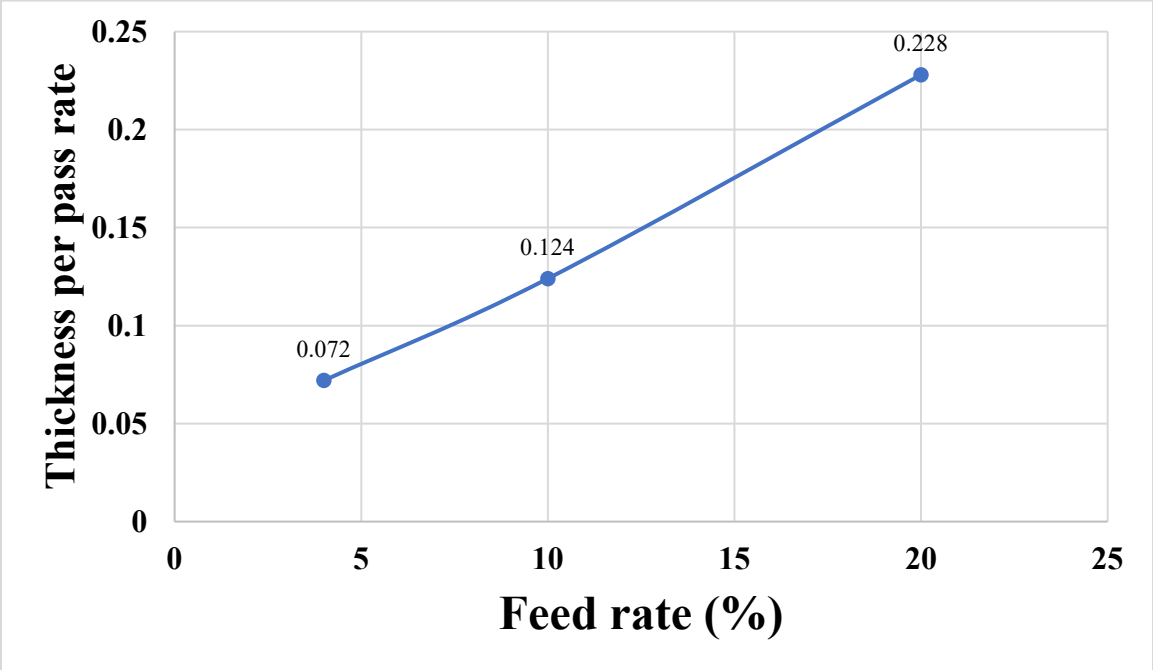

Figure 18. Feed Rate to Thickness-per-pass Rate Correlation at 40 mm/s.

b. Coating Porosity

Porosity of the trial specimens sprayed at 500 ºC and 1.38 MPa were also examined with the various spray conditions shown in Table 5. A porosity reduction trend was noted with an increase in feed rate and minimum number of passes as shown in Figure 19.

Table 5. Parameters of Spray Conditions at 500 ºC and 1.38 MPa for Porosity Investigation.

Spray Conditions	(a)	(b)	(c)	(d)	(e)	(f)
Carrier Gas Temp. (ºC)	500					
Carrier Gas Pressure (MPa)	1.38					
No. of Passes	4	4	2	2	2	2
Feed Rate (%)	4	6	15	15	20	20
Travel Speed (mm/s)	30	30	20	30	30	40

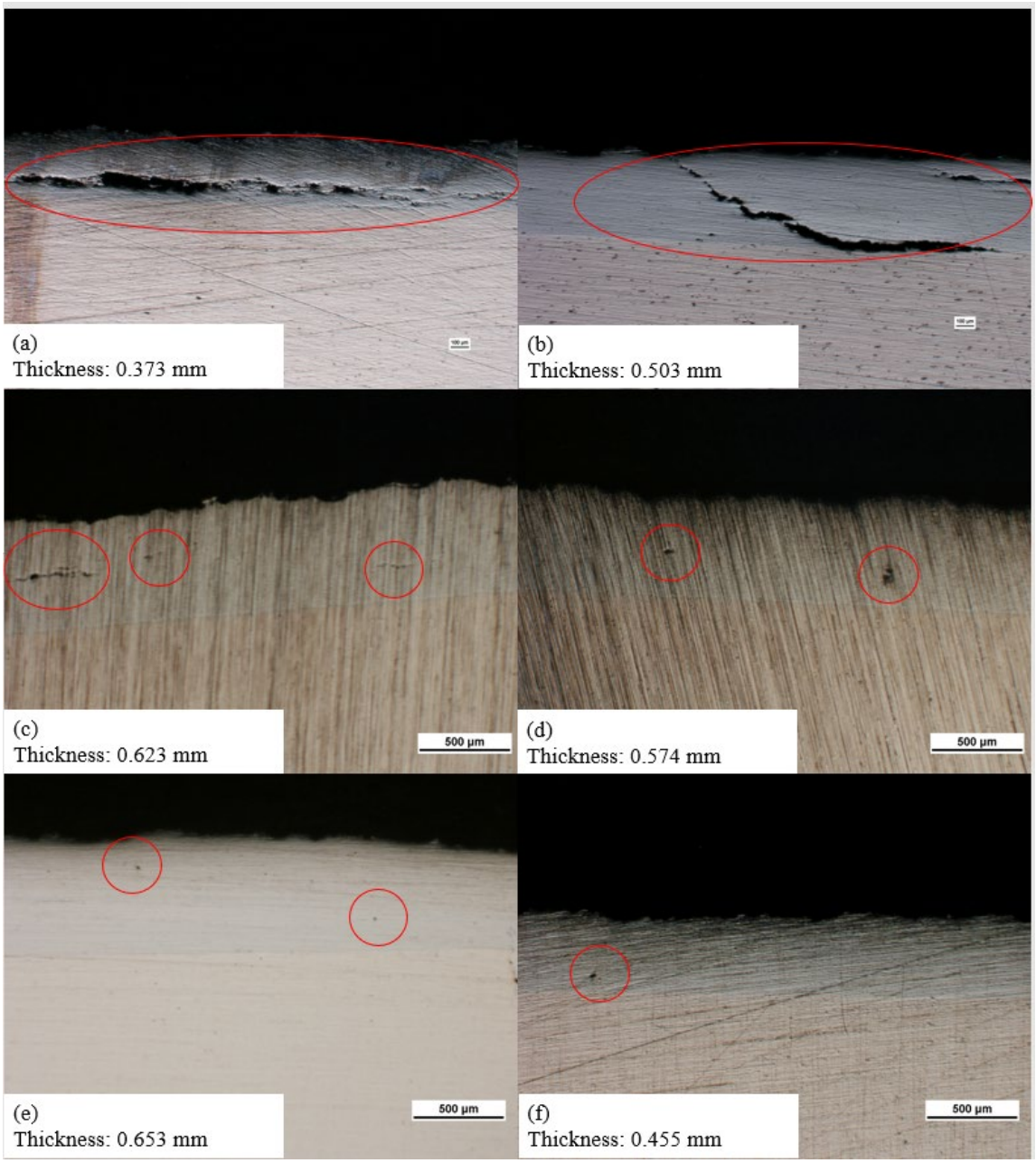

Figure 19. Porosity Reduction Trend with Increased Feed Rate and Minimum Number of Passes Vide Spray Conditions in Table 5. Visible Porosities are Circled in Red.

(1) High Pressure is Needed to Achieve Low Porosity and Thick Coating

While single-pass trials conducted with carrier gas at 500 ºC and 1.241 MPa were observed to have coherent coating-substrate adhesion, the coating performed with 10%

feed rate was observed with significant degree of porosity (Figure 20). The other observation was that the feed rate seems to be a more significant factor than number of passes to achieve thicker coating. Thus, the correlation between coating thickness and these factors are non-linear. The coating formed with 20% feed rate can well-compensate the doubling of passes with 10% feed rate by having thicker coating (0.436 mm for 20% feed rate in Figure 21 versus 0.393 mm for 10% feed rate in Figure 20).

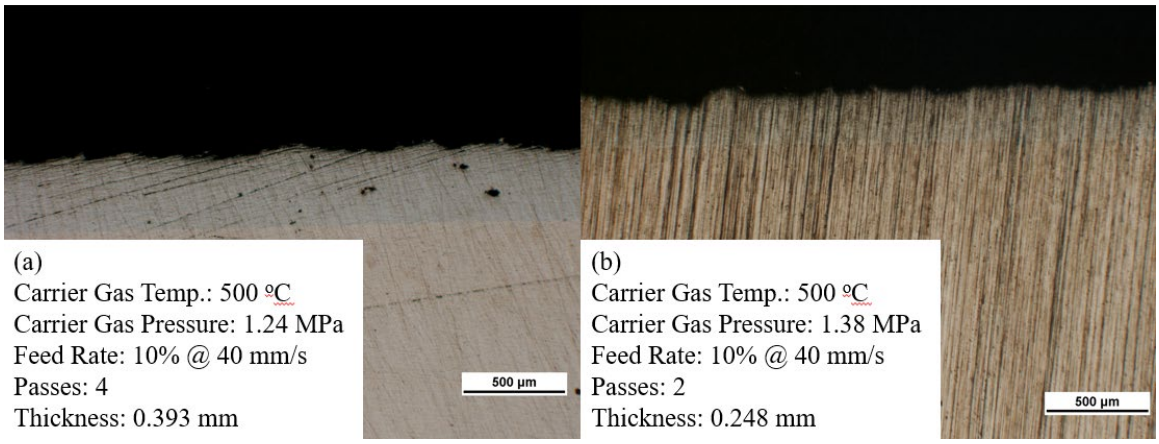

Figure 20. Coating Quality Comparison by Using Carrier Gas Pressure (a) 1.24 MPa, versus (b)1.38 MPa.

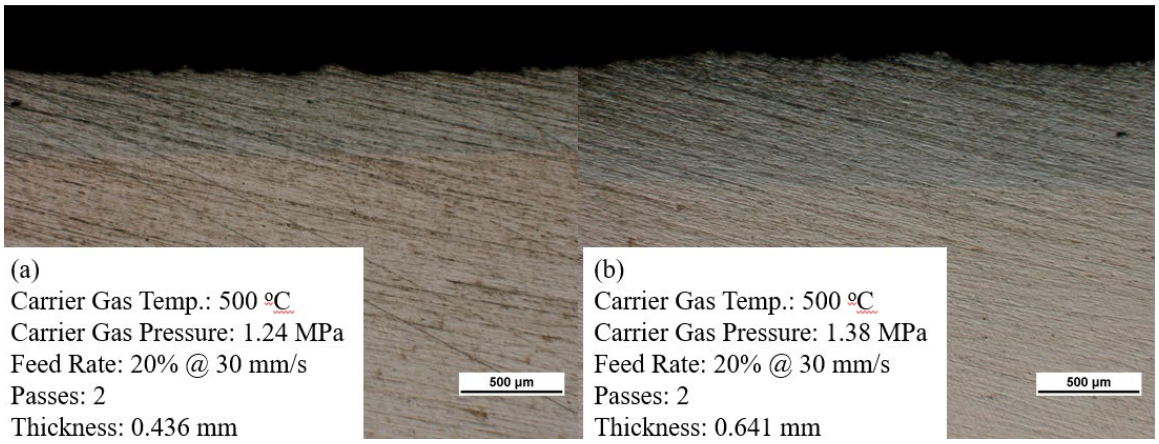

Figure 21. Coating Thickness Comparison by Using Carrier Gas Pressure (a) 1.24 MPa, versus (b)1.38 MPa.

(2) Matched Correlation of Coating Porosity with Carrier Gas Pressure, Number of Passes and Feed Rate

Porosity happens when the particles do not have adequate kinetic energy for plastic deformation and thermal softening to be flatten, which is necessary for mechanical interlocking at interfaces at minimum if not for metallurgical bonding. Oxides are documented to hinder adhesion at coating-substrate and coating-coating interfaces. Oxide film can possibly remain on the particles or substrate during the impact when the particles do not have enough energy to clear the oxide upon impact. Hence, the increase number of passes correspondingly increase the probability of oxide-hindered interfaces within the coating. These conventional understandings could had been validated that shows the reduction of porosity with (1) reduced the number of passes from four to two vide Figure 19, and (2) increased carrier gas pressure from 1.241 MPa to 1.379 MPa vide Figure 20. It was observed that the pores were less observed at the coating-substrate interfaces but predominantly within the coating. Of note, porosity was significant at the coating-substrate interface when feed rates were at 4% and 6%. Possible explanations could be (1) oxide film formed on the prior layer, or (2) reduced thermal softening of the prior layer coupled with its prior plastic strain hardening. The harder surface could rebound particles and resist the tamping effect. The lesser particles could also mean less metal jets to break adequate oxide film for adhesion to takes place and to form uniform layer. The higher carrier gas pressure translates to higher kinetic energy imparted to the ejected particles.

c. Coating Adhesion

J-B Weld Steel Reinforced Epoxy 8265S (tensile strength 34.61 MPa) was used during the trials. The parameters of the relevant spray conditions are summarized in Table 6. Firstly, the dollies of all spray conditions were observed with mixture of adhesive and coating failure, except for spray condition (c). Dollies of spray condition (c) were observed predominantly with adhesive instead. This is likely due to the visibly thin coating resulted from the travel speed of 50 mm/s. Hence, this set of readings is inconsequential. Secondly, the readings for spray condition (a) and (b) are of higher average values than those of spray condition (d) and (e). Moreover, the readings for spray

condition (a) and (b) are approximately close to the advertised tensile strength of 8265S. This droves the need to use Masterbond EP15ND-2 which has higher advertised tensile strength. The dollies for the respective spray conditions are shown in Figure 22 while the adhesion strength readings obtained are shown in Table 7.

Table 6. Parameters of Spray Conditions at 500 ºC and 1.38 MPa for Adhesion Investigation.

Spray Conditions	(a)	(b)	(c)	(d)	(e)
Carrier Gas Temp. (ºC)	500				
Carrier Gas Pressure (MPa)	1.38				
No. of Passes	1	1	1	2	2
Feed Rate (%)	4	4	5	15	15
Travel Speed (mm/s)	30	40	50	20	30

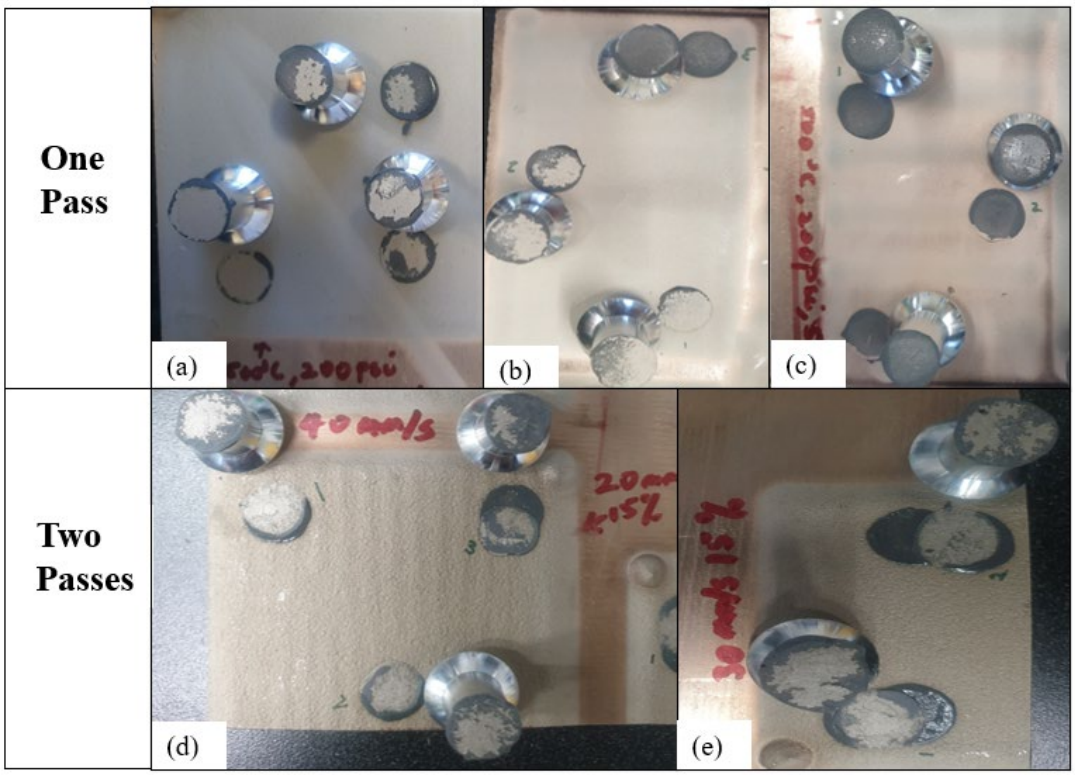

Figure 22. Post-Test Dollies for Respective Spray Conditions.

Table 7. Adhesion Strength Readings (MPa) from Trials Using 500 ºC and 1.38 MPa.

Spray Conditions / S/N	(a)	(b)	(c)	(d)	(e)
Average	35.54 ± 3.70	30.06 ± 4.57	30.27 ± 2.59	24.37 ± 4.65	22.33 ± 5.32
Observations	Mixture of adhesive and coating failure	Mixture of adhesive and coating failure	Adhesion failure, possibly due to thin coating formed by higher travel speed	Mixture of adhesive and coating failure	Mixture of adhesive and coating failure

(1) Stronger Coating-Substrate Adhesion vis-à-vis Coating-Coating Adhesion

Only spray condition (a) and (b) were observed with mixture of adhesive and coating failure. Considering the standard deviation of the readings and possible porosity in coatings, it would be possible for the higher stress experienced at the stress risers in the coating that led to the crack initiation on the coating until the cracks reached the coating-adhesive interface. The remaining smaller area of the effective coating-adhesive interface led to the eventual failure of 8265S. Thus, those higher readings from spray condition (a) were likely indicative coating-substrate adhesion strength and eventually failed when both critical crack length in coating and approaching of 8265S's UTS were met.

d. Optimal Spray Setting

Vide the prior paragraphs, the observable optimal setting to achieve coating thickness of approximately 9% of substrate thickness with proper coating adhesion and least porosity is postulated as (1) 500 ºC, (2) 1.379 MPa, (3) 30 mm/s, (4) 15% feed rate, and (5) two passes. As a result, further tests proceeded with the optimal set of parameters. Figure 23 shows the two sets of parameters with thick coating above 9% of substrate thickness.

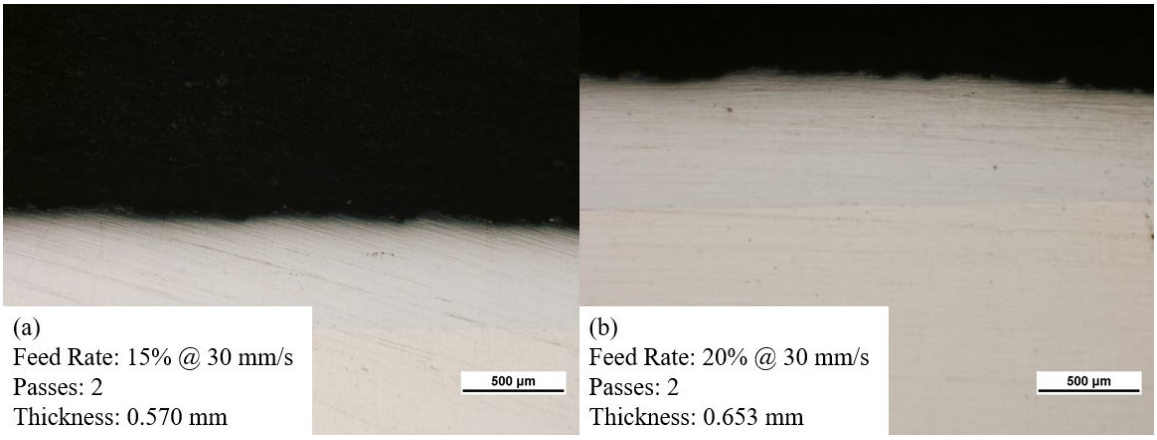

Figure 23. Comparison of Two Sets of Parameters with Thick Coating Above 0.57 mm (9% of Substrate Thickness).

2. Actual Experiment

Cu-38Ni powder was successfully cold-sprayed onto the grit-blasted Cu-10Ni plate per the defined optimal spray setting vide prior sub-section. In addition, a section with only single pass was sprayed for comparison. Heat treatment of the identified specimen groups was also done successfully. Of note, the coatings and specimens had noticeable color change from bronze to greyish after the heat treatment. Figure 24 shows the appearance of the four specimen groups. Table 8 summarized the thickness for the single and double passes coatings. Measurements were taken at two different zones for better statistical average representation. Of note, the coating thickness is thinner than that achieved during the trial. This highlights the significance of other factors besides those known that affects coating's quality and raise deep understanding needed to attain repeatable results. While the annealed coated indicated thicker coating, there isn't objective evidence to attribute the increased thickness due to heat treatment instead of probable coating variation. The relevant study only showed that heat treatment can densify the coating [23]. The result charts shown in subsequent sub-sections are based on the representative characteristic data after comparison to the statistic average and standard deviation.

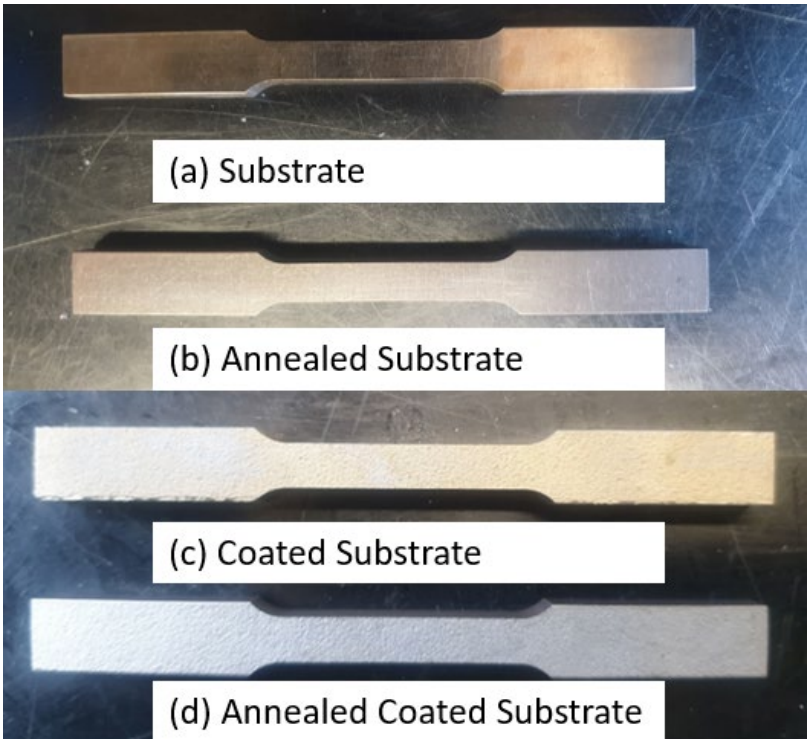

Figure 24. Appearance Comparison of All Specimen Groups.

Table 8. Actual Spray's Coating Thickness Measurements.

Unit of Measurement: µm	Single Pass	Coated (Double Passes)	Annealed Coated
Average	140.83 ± 17.07	432.40 ± 11.96	453.65 ± 15.47

From the etched cross-sectional view of the coating-substrate interface shown in Figure 25, it can be seen that (1) the coating particles were adhered to the substrate, and (2) splat microstructure is continuous with only small amounts or pores and inter-splat porosity. This feature was also observed from the SEM images of the fractured as-sprayed coating from the tensile test as shown in Figure 26.

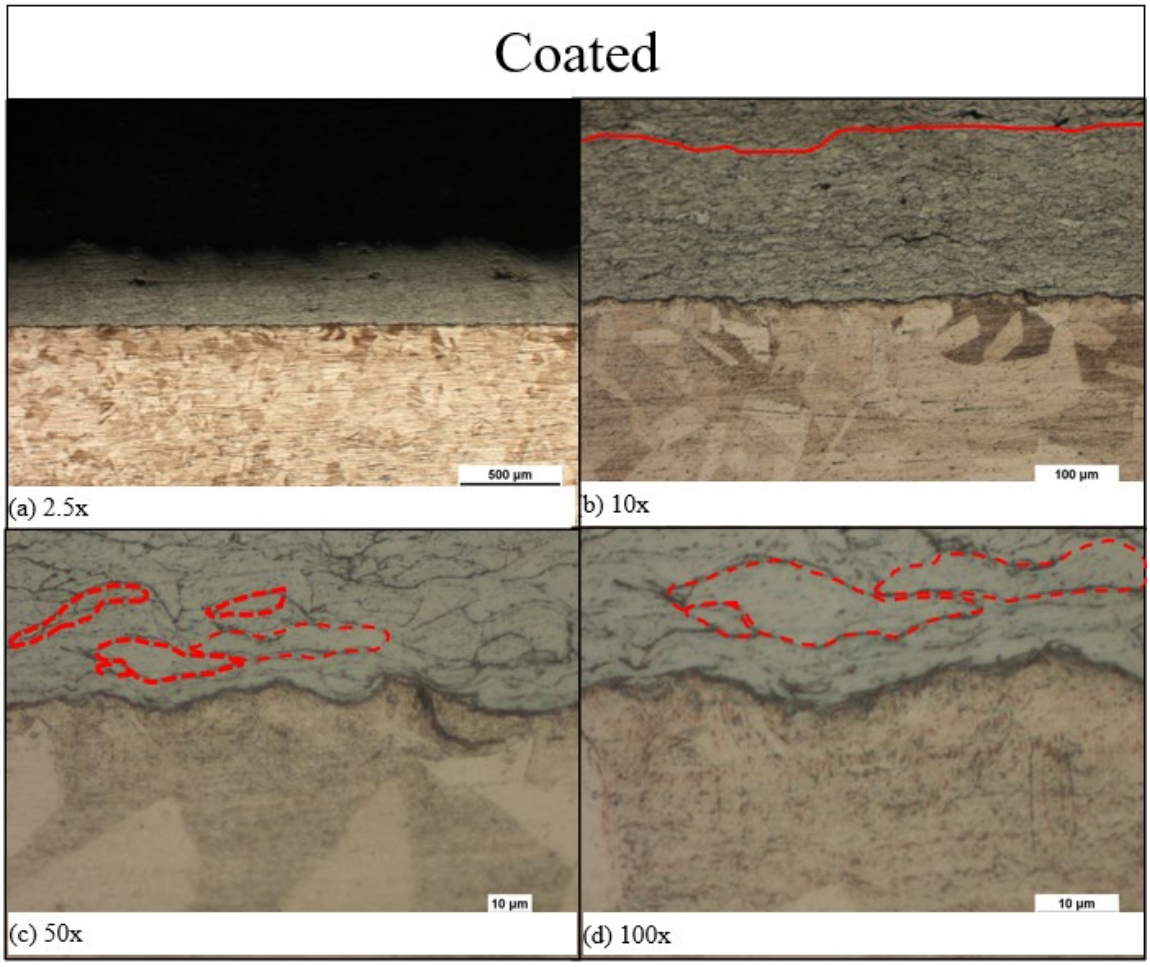

Figure 25. Splat Microstructure and Inter-Pass Interface Shown with Cross-Sectional Microscopic Images of Etched As-Sprayed Coating-Substrate Interface at Different Magnifications of (a) 2.5x, (b) 10x, (c) 50x, and (d) 100x. Some of the Splats are Highlighted with Red Dotted Lines. The Interface between the Two Passes is Distinguished by Porosity and Illustrated by the Offset Red Line.

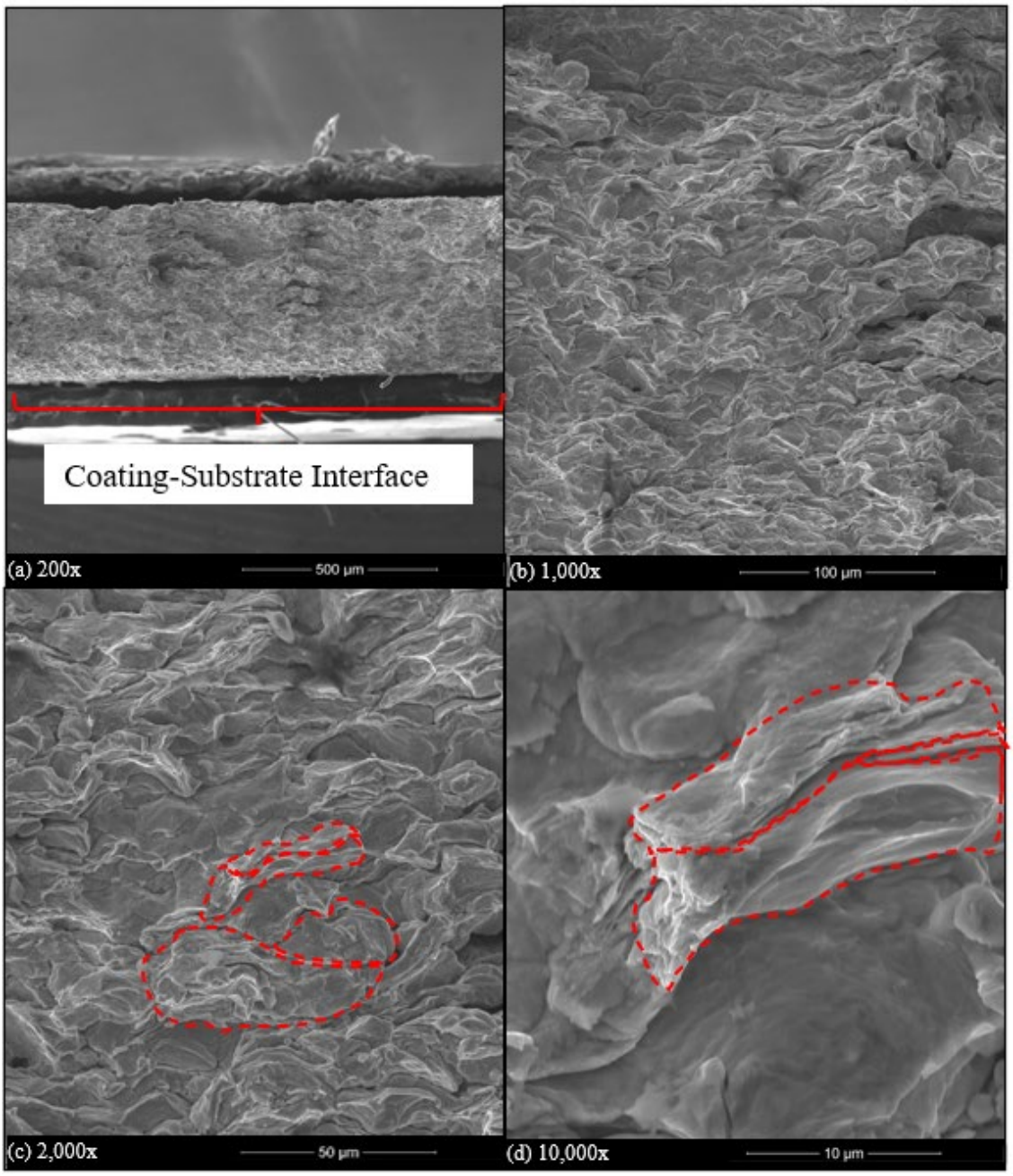

Figure 26. Splat Microstructure Shown with Cross-Sectional SEM Images of Fractured As-Sprayed Coating at Different Magnifications of (a) 200x, (b) 1,000x, (c) 2,000x, and (d) 10,000x.

a. Coating-Substrate Adhesion Strength

Distinct differences in the coating strength between the coated and annealed coated specimens were revealed through the adhesion test as shown in Figure 27. The coated specimens had average adhesion strength of 17.944 MPa. The 2nd pass coating was the predominant failure point during adhesion tests, with a partial portion of the 1st pass coating layer failing as well. Most of the 1st pass coating remained adhered to the substrate. This is supported by the slightly thicker 1st pass cohesive failure remnant coating against that of the single pass coating by 24 μm as shown in Table 9. The cross-sectional microscope image of the failed specimen shown in Figure 28 proved the stronger adhesion between the 1st pass coating and the substrate. The coating failure between 1st and 2nd pass coatings was likely due to the porosity present. In contrast, the annealed coated specimens had average tensile strength of 46.564 MPa with the coatings remained intact. The adhesive was the weaker material than the annealed coating. Although the coating's adhesion strength was not determined, this result indicated with confidence that the annealed coating is stronger than 46.564 MPa. Table 10 summarized the adhesion test measurements.

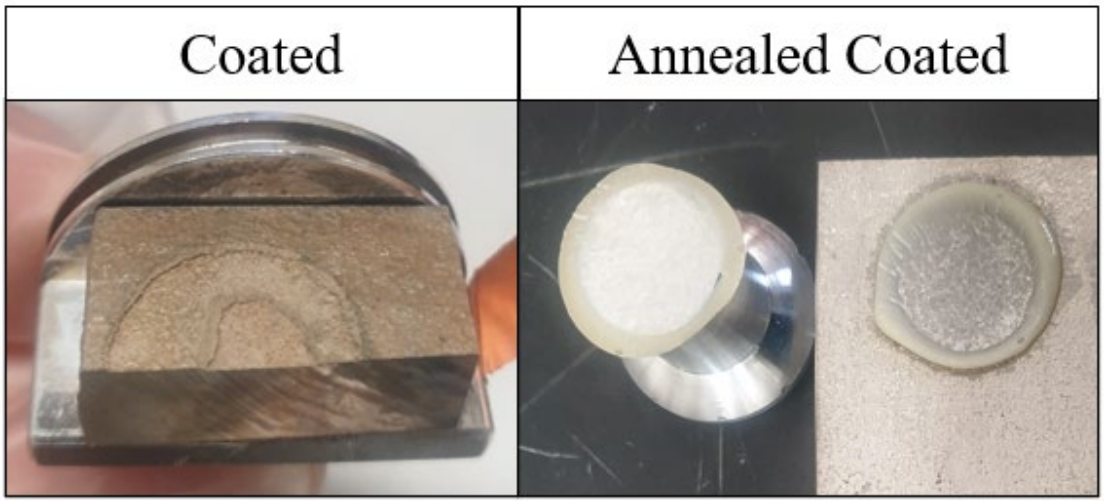

Figure 27. Adhesion Test Failure Comparison between (a) Coated Specimen, and (b) Annealed Coated Specimen.

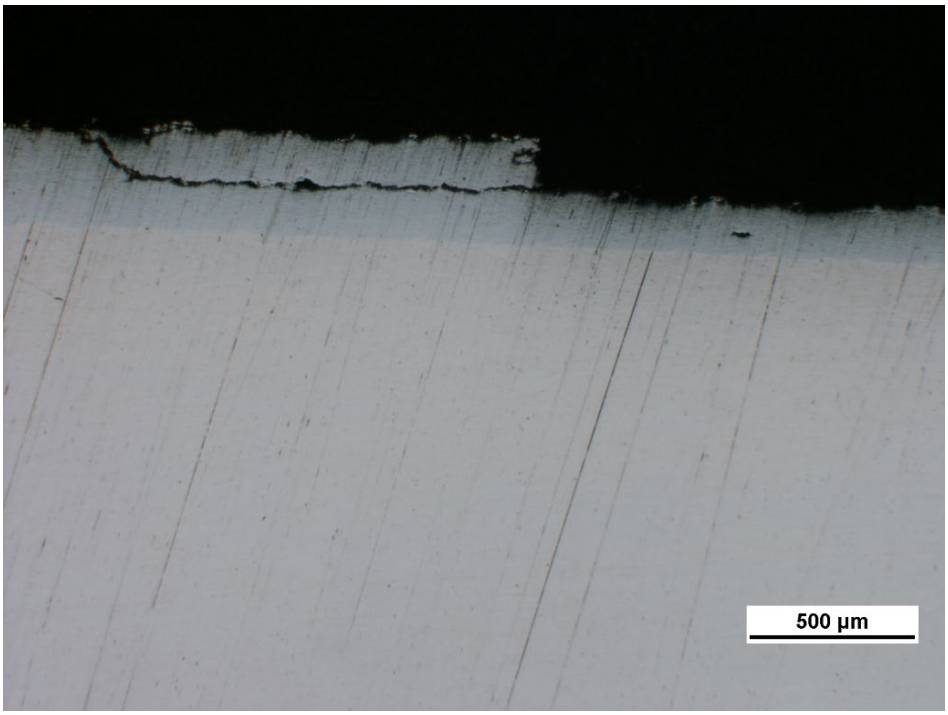

Figure 28. Cross-Sectional Microscope Image of Failed Coating on Coated Specimen.

Table 9. Thickness Comparison between Single Pass and Remnant 1st Pass Coatings.

Unit of Measurement: µm	Single Pass	Remnant
Average	140.83 ± 17.07	164.69 ± 8.13

Table 10. Specimens' Adhesion Strength Measurements.

	Average (MPa)	Observations
Coated	17.94 ± 2.80	Coating failed
Annealed Coated	46.56 ± 0.67	Masterbond failed

b. Specimens' Tensile Strength

There were three distinct mechanical behavior differences amongst the four specimen groups observed from the tensile testing, with Figure 29 shows the coatings' failure appearances. Firstly, with reference to the substrate group, cold spray had cold-

work effect to strengthen the substrate while reduced its ductility that is evidence by the shorter rupture displacement. Secondly, the as-sprayed coating was brittle and delaminated from the substrate at low tensile strength at approximately 6,416 N or 149.37 MPa (see Figure 30). Lastly, heat treatment evidently changes the mechanical behavior of the coating in three aspects: (1) restored ductility in coating with visible cracks started to form approximately 11 kN or 268.22 MPa onwards, (2) increased UTS and YS at the expense of reduced ductility in the substrate, and (3) improved coating-substrate adhesion.

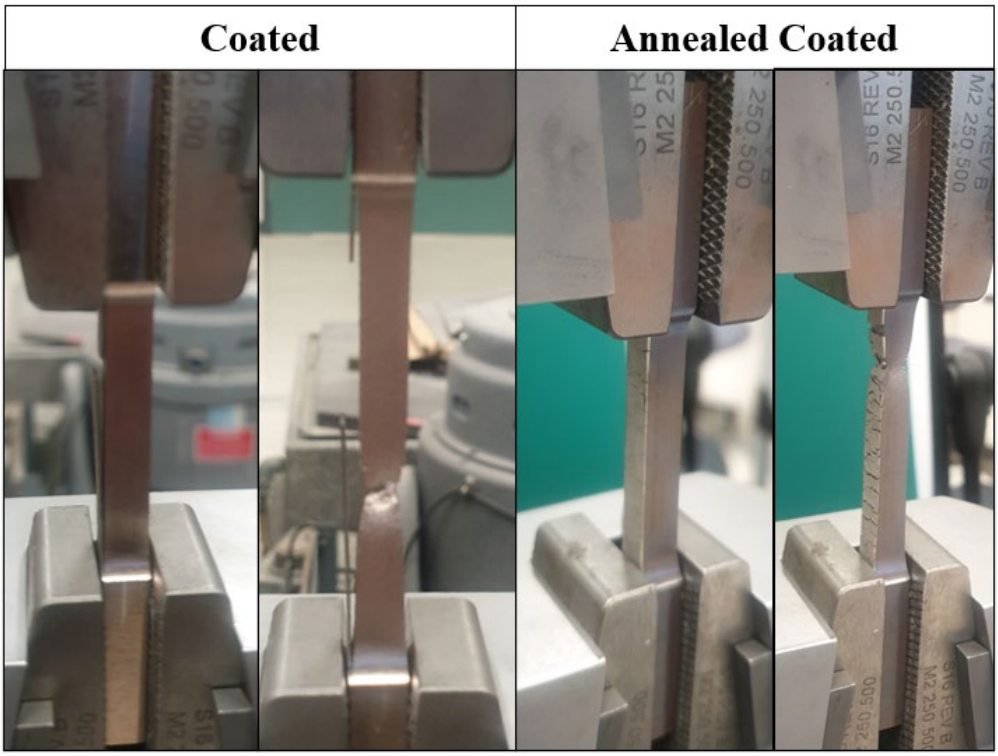

Figure 29. Difference in Coating Failure for Coated and Annealed Coated.

The coating failure represents the change in the effective cross-sectional area and hence the corresponding stress experienced by the specimen. The averaged total coated cross-sectional area and substrate's original cross-section area per ASTM E8/E8M – 09 standard were used for close approximation of the actual stress experienced by the specimens prior and after the coating's failure. The strain and stress values are calculated

based on the load response plots shown in Figure 30 in conjunction with Equation (2) and (3). Of note, the coatings' failure for the coated specimens are pronounced on the chart due to the abrupt rupture of the coating. In comparison, the coatings' failure for annealed coated specimens are only pronounced in two out of five of the specimens. The crack initiation point for the remaining three specimens were hence undefined. Table 11 summarized the indicative coating rupture loads for each of the specimen groups. The load responses charts for the filmed coated and annealed coated specimens based on the known crack initiations on the coatings are shown in Figure 31, which presented the difference in the cyclic feature of the load responses. The continuous cyclic loading with no drastic change could be representing the multiple crack initiations across the well-adhered annealed coating observed. Figure 32 shows the characteristic stress-strain plots of the actual response for all specimen groups and Table 12 summarized the specimens' final rupture displacement and maximum load measurements. Elongation-to-rupture was calculated based on the known specimen original length of 3.206×10^{-2} m and in accordance with Equation (4). The elongation-to-rupture results are included in Table 12.

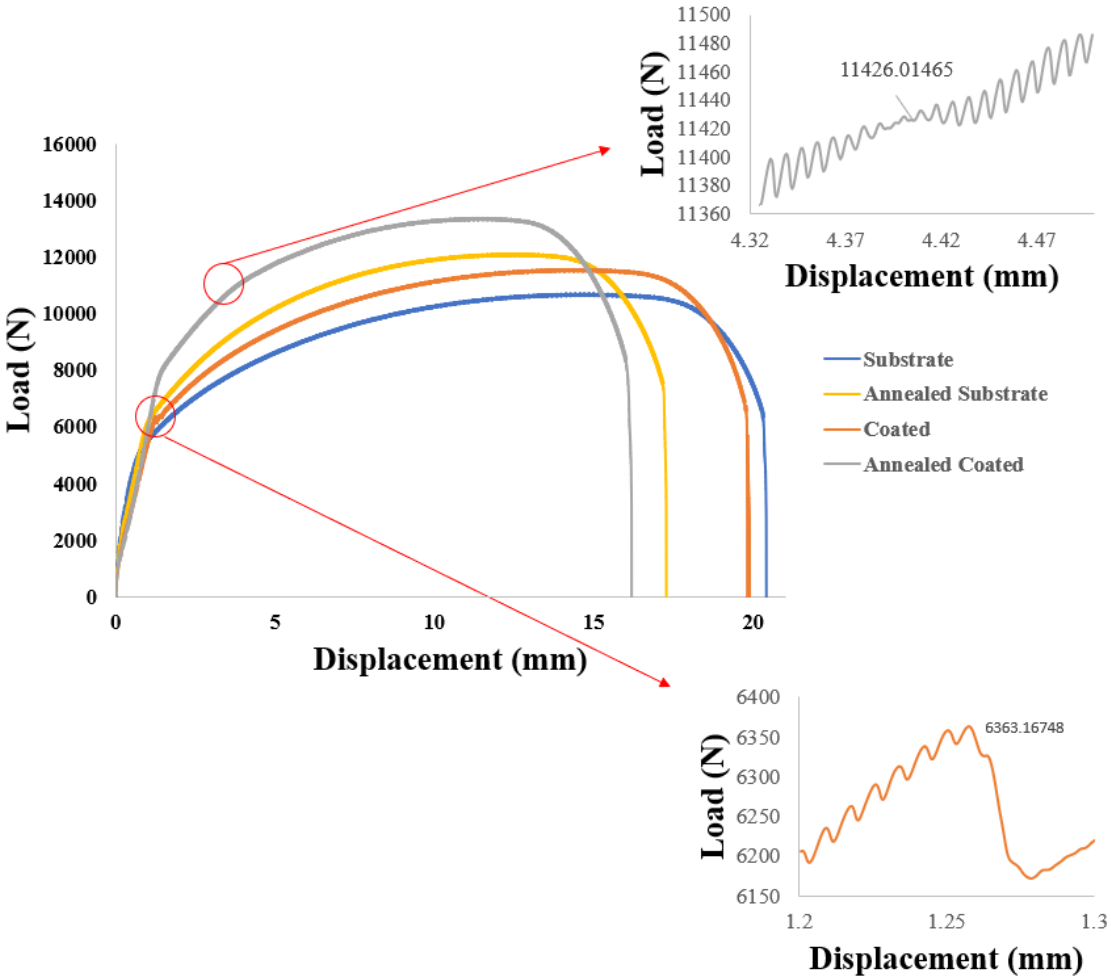

Figure 30. Representative Load-Displacement Plots for All Specimen Groups. The Maximum Load Sustained by the Specimens Represent the UTS, while the YS can be Inferred with 0.2% Displacement Offset from the Linear Portions Referenced from MMPDS [4]. The Pronounced Disruption in the Load-Displacement Response for Coated (Bottom) and Annealed Coated (Top) Specimens are Highlighted.

Table 11. Indicative Coatings' Rupture Load Measurements.

Specimen Groups		Average
Rupture Load (N)	Coated	6,415.98 ± 122.08
	Annealed Coated	11,955.47 ± 529.45

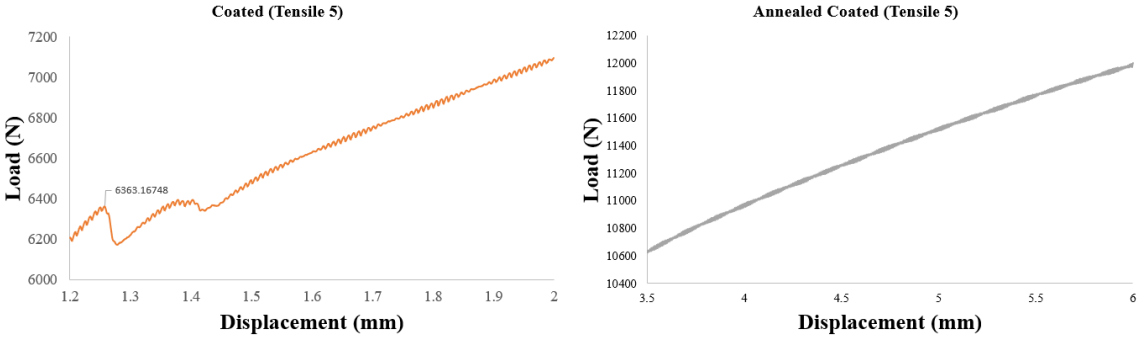

Figure 31. Difference in Load-Displacement Plots for Coating Failure of (a) Coated, and (b) Annealed Coated.

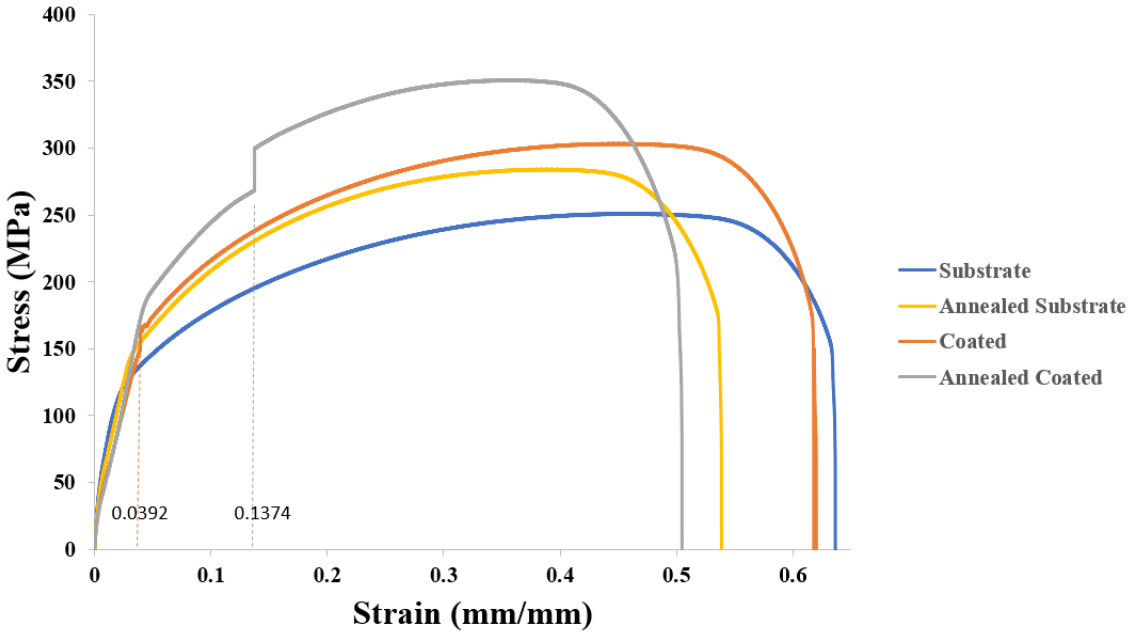

Figure 32. Representative Characteristic Stress-Strain Plots of Actual Response for All Specimen Groups. The Maximum Stress Sustained by the Specimens is Indicative of Their Ultimate Tensile Stress Capability, while Their Indicative Yield Stress Capability can be Inferred with 0.2% Strain Offset from the Linear Portions referenced from MMPDS [4].

Table 12. Specimens' Final Rupture Displacement and Maximum Load Measurements, with Elongation to Rupture.

Specimen Groups		Average
Substrate	**Rupture Displacement (mm)**	20.38 ± 0.27
	Elongation-to-Rupture (%)	63.56 ± 0.85
	Max. Sustained Load (N)	10,653.84 ± 83.03
Annealed Substrate	**Rupture Displacement (mm)**	17.20 ± 0.22
	Elongation-to-Rupture (%)	53.65 ± 0.68
	Max. Sustained Load (N)	11,940.31 ± 133.61
Coated	**Rupture Displacement (mm)**	19.82 ± 0.29
	Elongation-to-Rupture (%)	61.83 ± 0.91
	Max. Sustained Load (N)	11,616.04 ± 86.14
Annealed Coated	**Rupture Displacement (mm)**	16.08 ± 0.23
	Elongation-to-Rupture (%)	50.15 ± 0.71
	Max. Sustained Load (N)	13,264.36 ± 171.95

c. Coating and Substrate's Young's Modulus and Hardness

Minimum of 27 indentation results were obtained for each of the substrate, annealed substrate, as-sprayed coating, and annealed coating to obtain the correspond regions' Young's modulus and hardness. Plasticity, elastic recovery and contact stiffness are variables used by Nanoindenter G200 to derive the Young's modulus and hardness, and can be estimated from the plots in Figure 33. Table 13 summarized the derived Young's modulus and hardness of the respective specimen regions by Nanoindenter G200, as well as the estimated plasticity.

The plots in Figure 33 reiterated the similar observations from the tensile tests pertaining the respective specimens' ductility based on their maximum displacements. Cold spray is experimentally proven to have cold-work hardening effect which can be alleviated through heat treatment. Heat treatment is also shown to strengthen the specimens with the corresponding higher Young's modulus which relates to higher required stress to result in strain. Of note, as-sprayed coating is estimated to have the lowest plasticity and highest hardness. These relativity properties substantiated the as-sprayed coating's brittleness. In addition, as-sprayed coating has higher Young's modulus

than the substrate. This is due to the difference in their Cu-Ni compositions. It is also noted that heat treatment had more improvement on the substrate's Young's modulus than that of the coating.

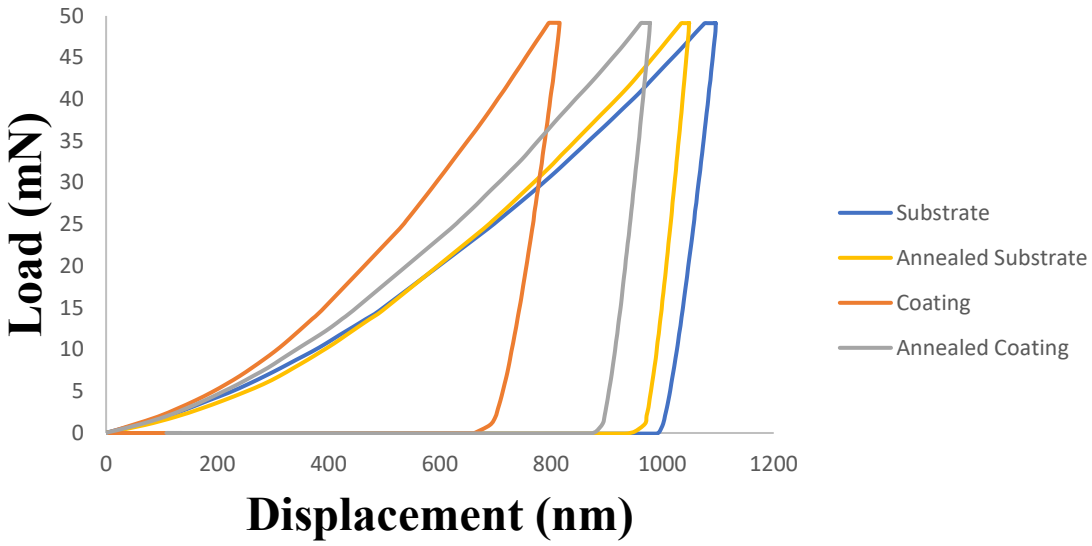

Figure 34. Nanoindentation Load-Displacement Plots for All Specimen Groups.

Table 13. Specimens' Nanoindentation Measurements.

	Substrate	Annealed Substrate	Coating	Annealed Coating
Plasticity %	90.24	88.95	81.10	89.12
Average Young's Modulus (GPa)	104.26 ± 6.00	132.06 ± 6.82	120.70 ± 11.28	134.29 ± 9.27
Average Hardness (GPa)	1.74 ± 0.33	1.90 ± 0.16	3.32 ± 0.48	2.24 ± 0.25

B. DISCUSSIONS

1. Cu-38Ni Powder Requires High Kinetic Energy for Metallurgical Bonding

The observed delamination of the as-sprayed coating during the tensile test suggested the adhesion between the coating and substrate is weak. SEM images of the

substrate's interface with the coating in Figure 34 showed probable islands of coating remnant. In addition, the etched cross-sectional images in previously shown Figure 25 revealed the observable black interface line between the coating and substrate. This observation suggested either the presence of oxide film or absence of metallurgical bonding as evident on the coating itself. Furthermore, observable interlockings between splats are seen in Figure 26 which could be the similar observation by Li et al. [33]. Thus, it is postulated that mechanical interlocking is the predominant adhesion type between the as-sprayed coating and substrate. This hypothesis is based on Yin et al. [7] whom mentioned metallurgical bonding being stronger than mechanical interlocking. This prompted that further parameters optimization is required to provide the coating particles with additional energy to form metallurgical bonding instead.

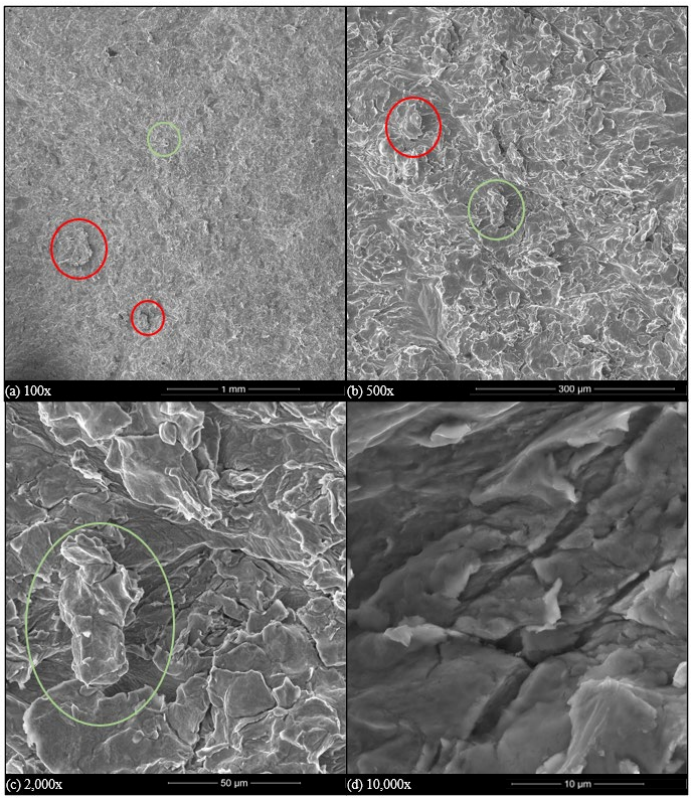

Figure 35. SEM Images of Coating Remnants on Substrate at Different Magnifications. Green circles provided the relative position of the particular coating remnant with respect to the other coating remnants observed that are in red circles.

2. Heat Treatment Mitigated Mechanical Deficiencies Associated with Porosity

Heat treatment was proven to be a critical post-processing route to mitigate mechanical deficiencies associated with the porosity present in the coated. In comparison of the load-displacement results between the coated and annealed coated specimens, it is evident that heat treatment increases the maximum sustained load by approximately 14.2% at the expense of 18.9% ductility reduction. The UTS and YS increment could be due to the metallic bonding induced at the inter-splat boundaries as the heat treatment temperature of 650 ^{o}C is approximately 52% for Cu-38Ni and 58% for Cu-10Ni's of their respective melting temperature, well above the 40% to 50% thermal recrystallization criteria mentioned by Kumar et al. [27]. SEM images comparison of the substrate fracture surfaces and resulting deformation mechanisms in Figure 35 and Figure 36 showed that the substrate exhibited a ductile response despite the cold spray or heat treatment applied. The annealed coating was proven to have adhesion tensile strength above 46.56 MPa without coating failure while the as-sprayed coating failed at 17.94 MPa. The annealed coating was found to have higher plasticity, hence further proven its higher ductility, and lower hardness than the as-sprayed coating. Of note, the coating and annealed coating consistently have higher hardness than their adhered substrates. This finding is likely attributed to particles' strain hardening upon impact and the tamping effect of both high-velocity impacted and rebounded particles as mentioned by Bae et al. [29]. The reduction of hardness and Young's modulus of the annealed coating could be due to the solid-state diffusion between inter-splat cracks that reduces the inter-splat crack density [36], [31].

The comparison of as-sprayed coating and annealed coating shown in Figure 37 appeared to possibly reveal the presence of a finer grain structures within the splats, and the inter-splat boundaries between individual coating particles became less discernible after the heat treatment. Similar observations near the pores in the coating are shown in Figure 38. Comparison at higher magnifications using the SEM were made. Figure 39 affirming the (1) densified coating with less inter-splat porosity, and (2) signs of solid-state diffusion at the coating-substrate interface. Figure 40 affirmed the signs of solid-

state diffusion within the annealed splat. The finer grains observed could also indicated recrystallization that occurred during the heat treatment, referencing to ultrafine grains in Ni-coating's particle-particles boundaries formed by dynamic recrystallization as mentioned by Zou et al. [32]. However, further inspection using transmission electron microscopy or electron back scatter diffraction is required to verify the presence of recrystallized grains and grain size. Finer grains formed from recrystallization are known to becomes weaker and more ductile [5]. This is validated with the nanoindentation results. However, the strength loss in individual grain can be negated by the solid-state diffusion between these finer grains that results in the coating's overall strength improvement. The less prominence of splat boundaries is likely evident of the solid-state diffusion energized by the thermal energy provided that reduces porosity, with reservation that the etched images' quality is also subjectivity to the etching process. The relative ductile failure of the annealed coating observed from the tensile test matched the similar observation by Silvello et al. [35] that less porous coating resulted in the pronounced ductile fracture in which can positively inhibited crack propagation.

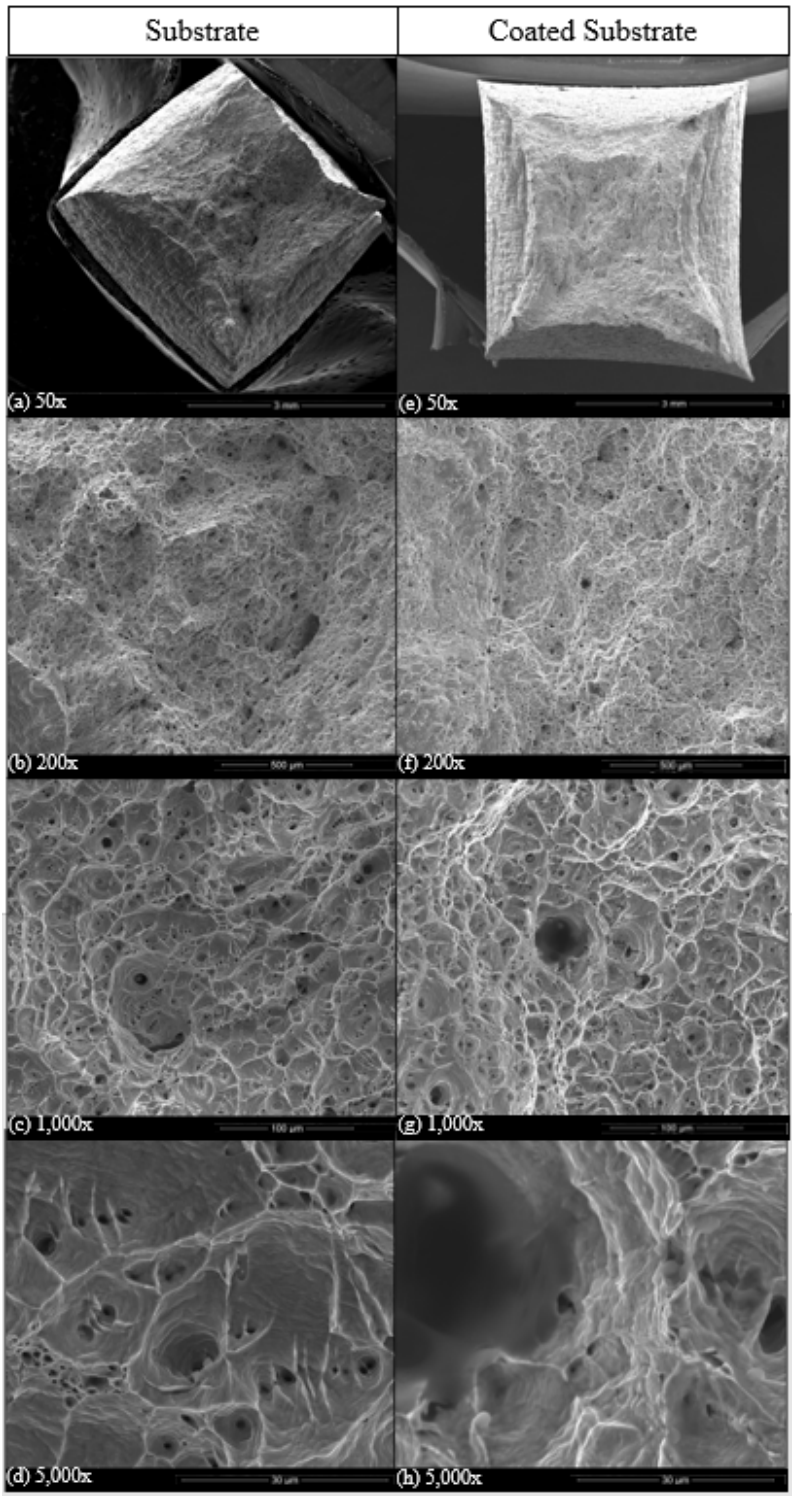

Figure 36. SEM Images Comparison of Fracture Surface at Different Magnifications for Substrate (a-d), and Coated Substrate (e-h). Ductile Features on Both Specimens.

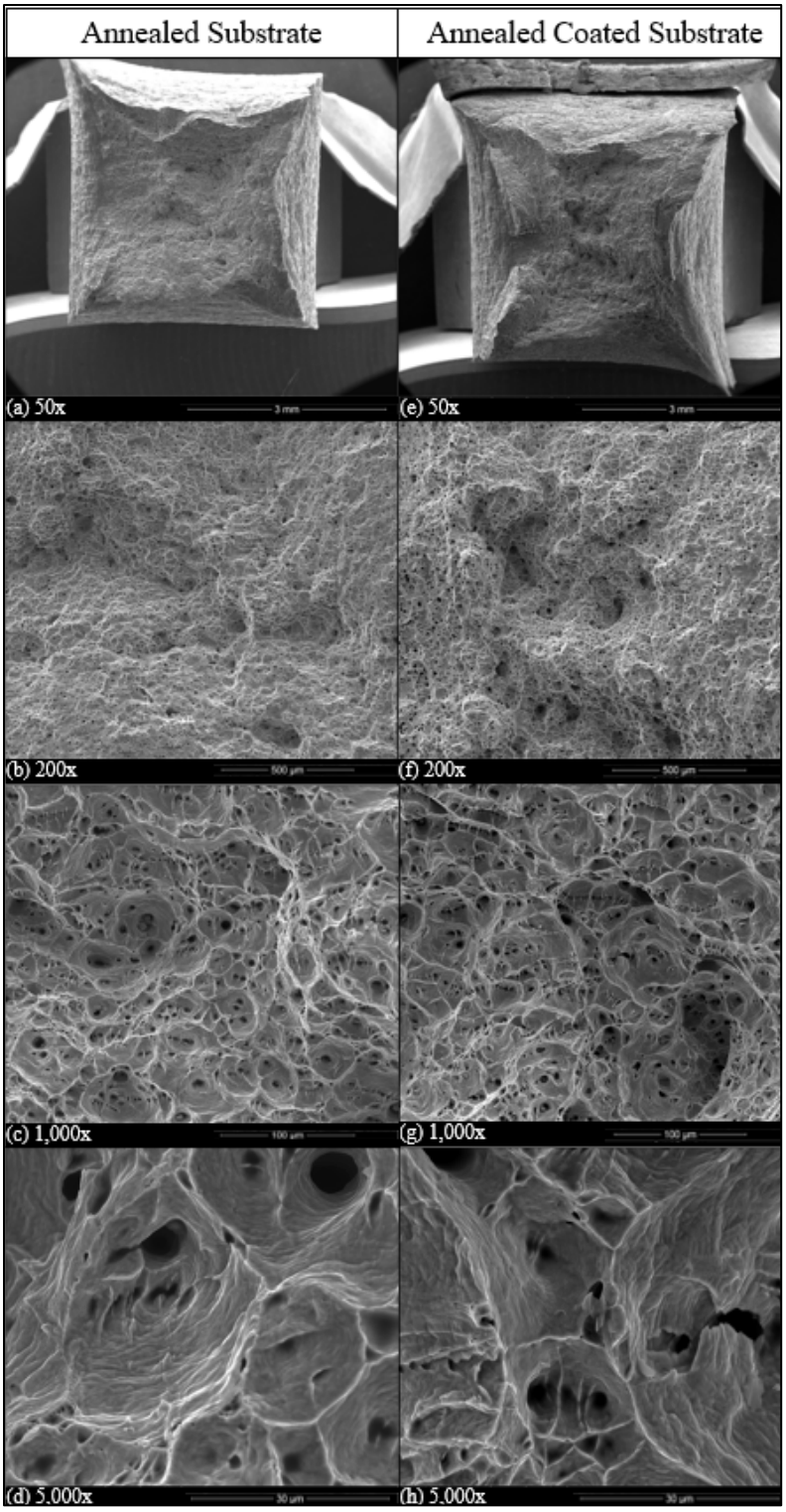

Figure 37. SEM Images Comparison of Fracture Surface at Different Magnifications for Annealed Substrate (a-d), and Annealed Coated Substrate (e-h). Ductile Features on Both Specimens.

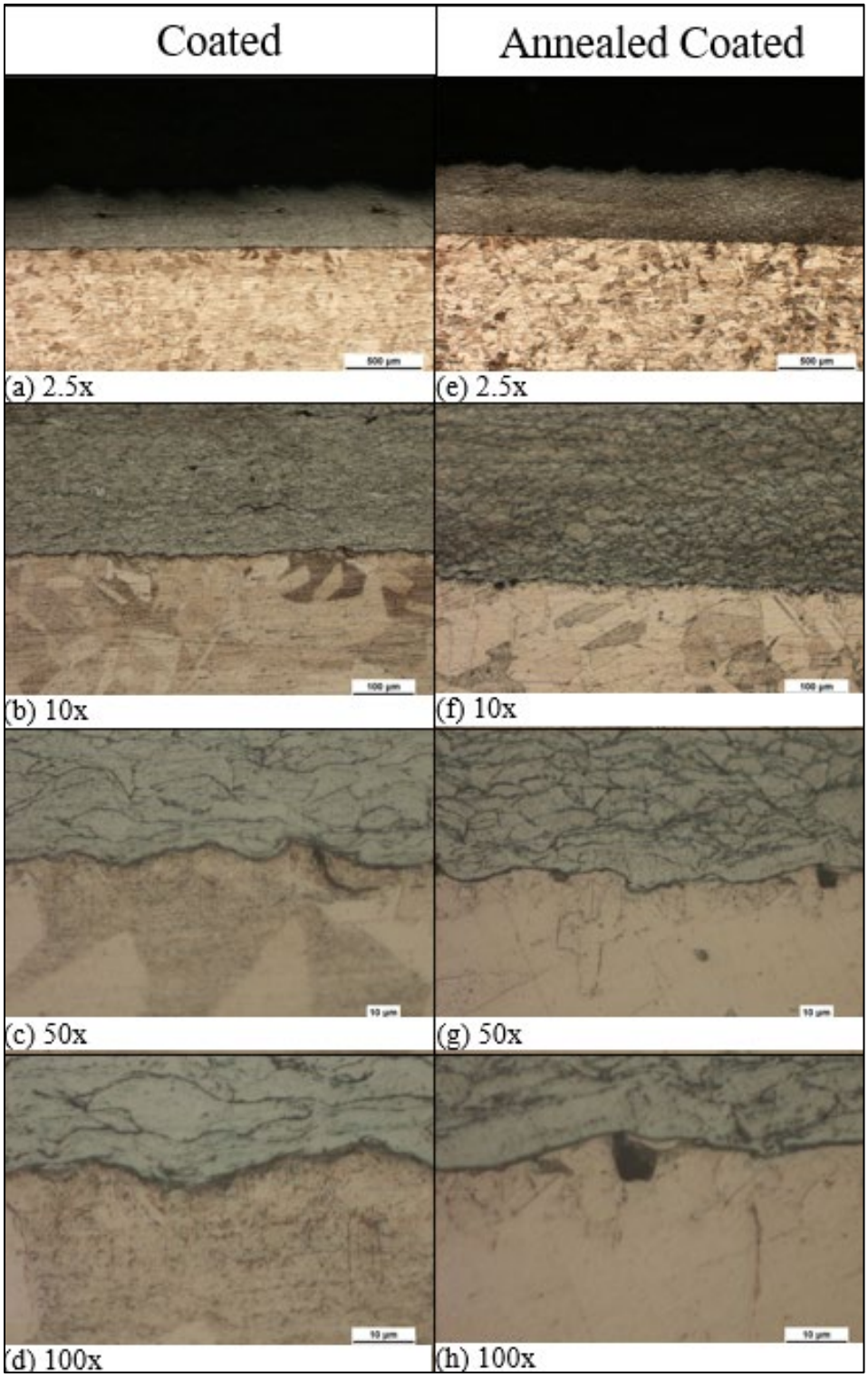

Figure 38. Microscopic Image Comparison of Etched Coating-Substrate Interfaces at Different Magnifications for Coated Specimen (a-d), and Annealed Coated Specimen (e-h).

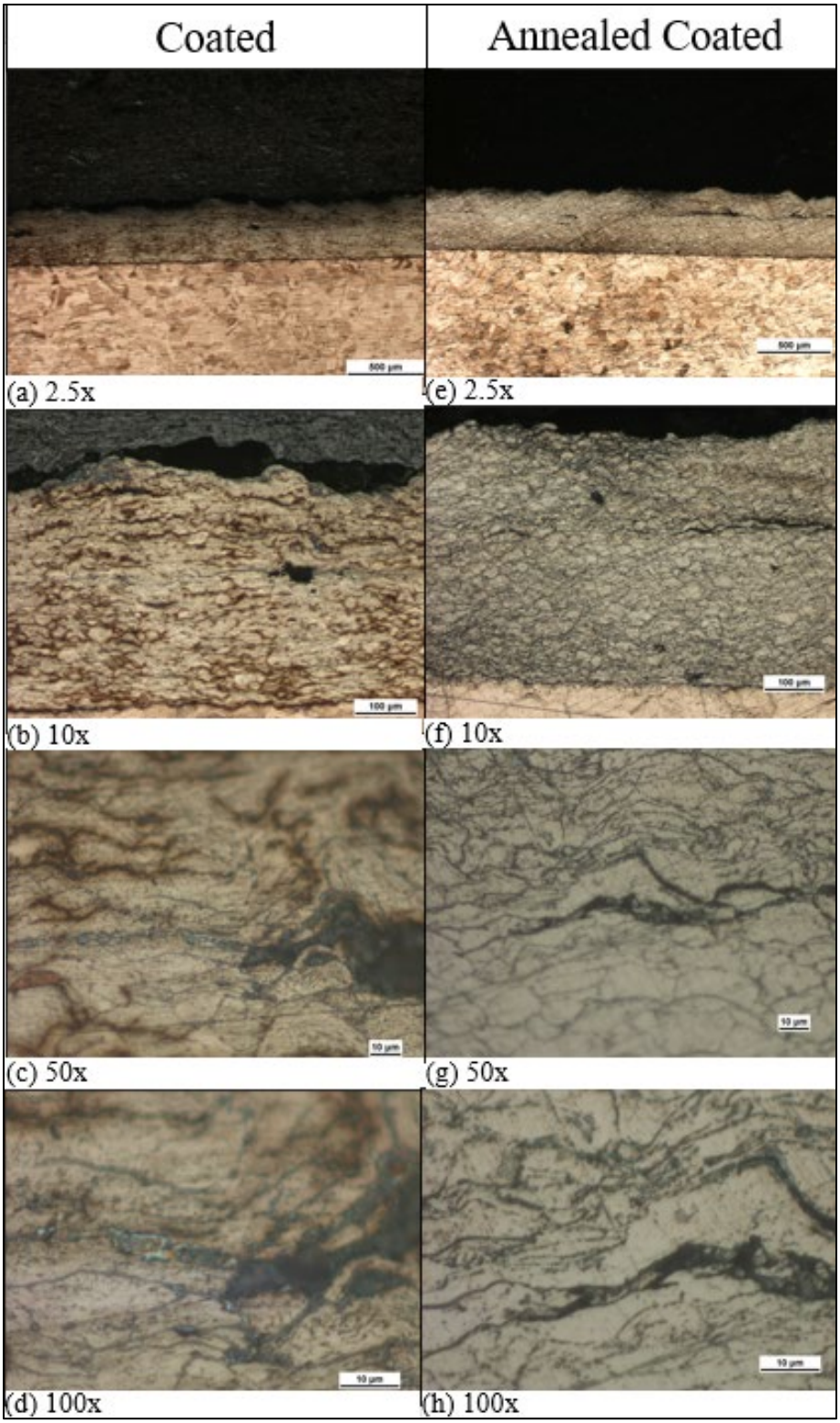

Figure 39. Microscopic Image Comparison of Etched Passes Interfaces at Different Magnifications for Coated Specimen (a-d), and Annealed Coated Specimen (e-h).

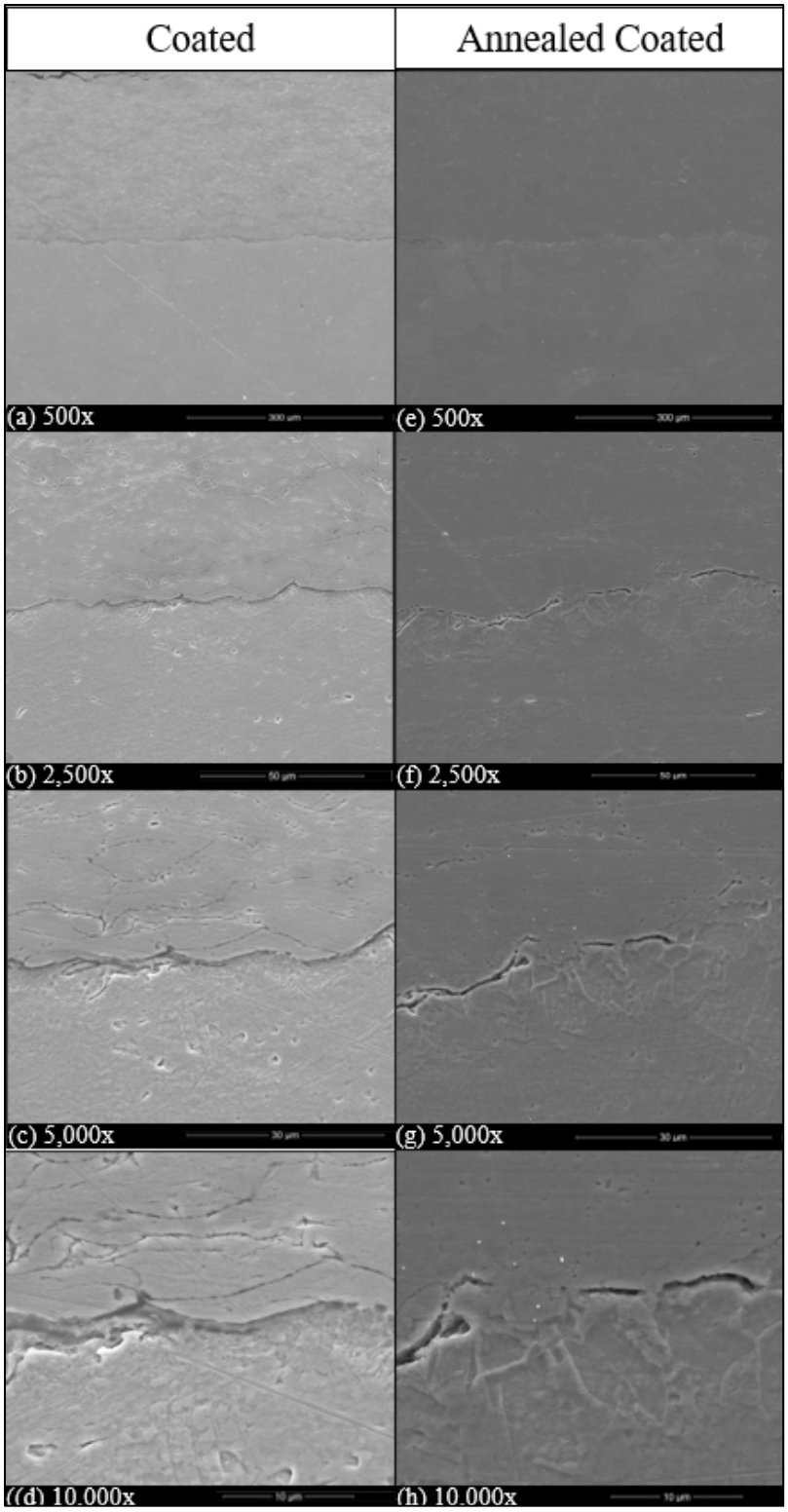

Figure 40. SEM Images Comparison of Etched Coating-Substrate Interfaces at Different Magnifications for Coated Specimen (a-d), and Annealed Coated Specimen (e-h).

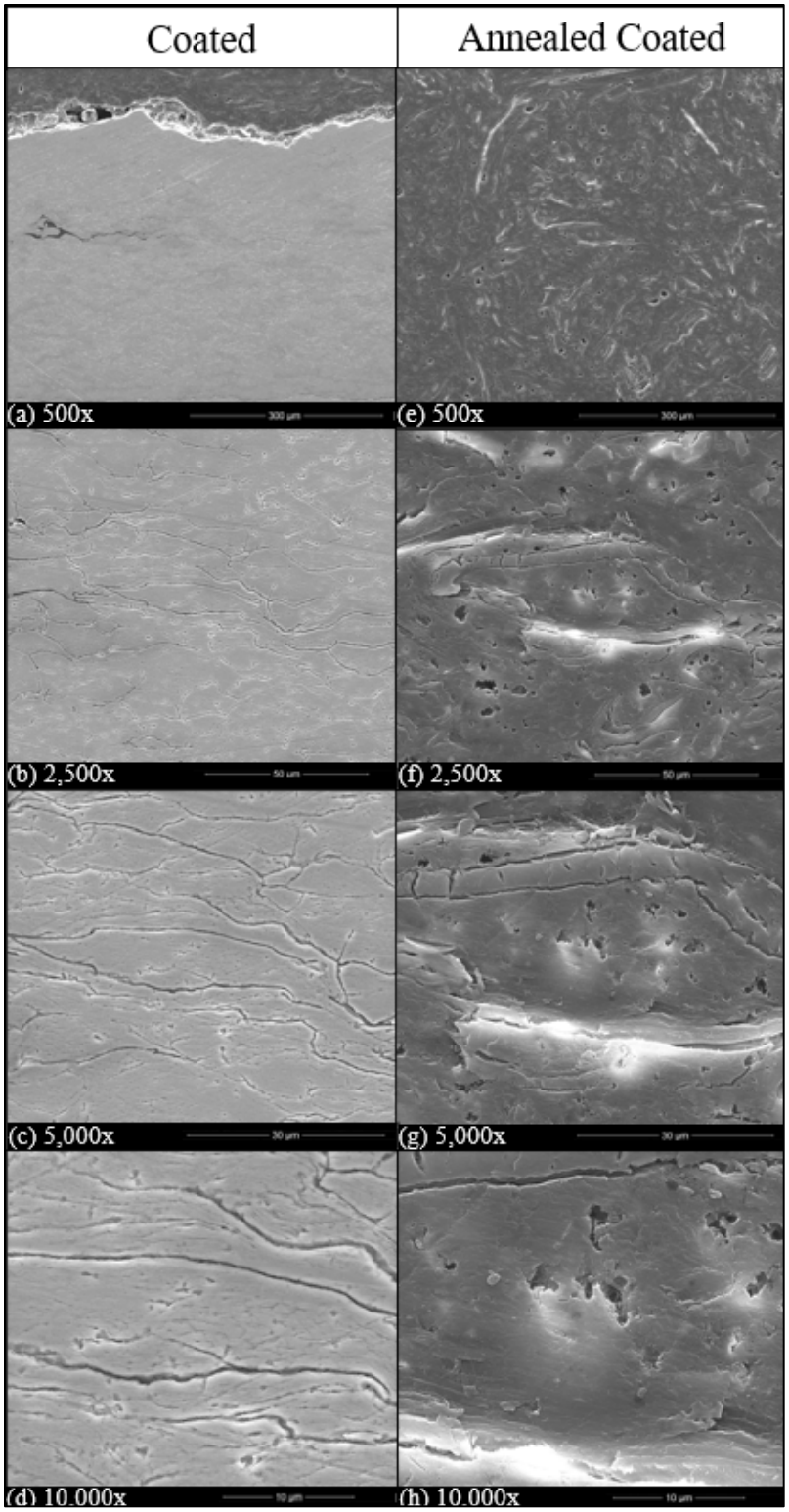

Figure 41. SEM Images Comparison of Etched Splats at Different Magnifications for Coated Specimen (a-d), and Annealed Coated Specimen (e-h).

IV. CONCLUSION

A. KEY TAKEAWAYS

Cold spray can effectively cold-work the substrate to strengthen its tensile strength and adhere the intended coating particles onto the substrate to a desired thickness. The optimal combination of high carrier gas pressure, high carrier gas temperature, high feed rate are main contributors for good adhesion. Porosity in the coating was evidently shown to deteriorate its mechanical behavior. Heat treatment is an effective strengthening mechanism that can mitigate the mechanical deficiencies that porosity poses. Annealed coating resultantly had stronger adhesion to its substrate. Annealed coating itself can bear significant load and strengthen the substrate. Nanoindentaion results show that heat treatment increased plasticity and reduced hardness of the coating to exhibit relative ductile behavior than the as-sprayed coating. Thus, cold spray coating with appropriate post-processing treatment can potentially reinforce and even repair component to achieve robust mechanical behavior.

B. FUTURE WORK

Further investigation may consider the use of helium as carrier gas that could further improve the as-sprayed coating's mechanical behavior as the coating particles would possess more average energy for forming metallurgical bonding. This might be a viable alternative to heat treatment which constraints in-field applications. Further investigation may also consider to explore parametric investigation spray parameters to achieve desired thick coating in one pass or resolve porosity between layers. Lastly, further investigation may continue this thesis's work to investigate the fatigue and corrosion performance of the Cu-Ni coating.

THIS PAGE INTENTIONALLY LEFT BLANK

APPENDIX A. TRIAL'S COATING THICKNESS MEASUREMENTS

Carrier Gas Temp. (^{o}C)	500									
Carrier Gas Pressure (MPa)	1.24		1.38							
No. of Passes	4	2	4	2	4	2	2	2	2	2
Feed Rate (%)	10	20	4	4	6	10	15	15	20	20
Travel Speed (mm/s)	40	30	30	40	30	40	30	20	30	40
Measurement 1 (µm)	0.39569	427.552	362.6	125.008	486.325	262.583	608.228	626.997	655.797	460.703
Measurement 2 (µm)	363.371	449.29	380.502	166.065	499.156	176.254	558.15	597.721	684.821	425.049
Measurement 3 (µm)	410.077	460.145	370.312	154.468	514.902	287.852	568.883	644.532	648.551	467.859
Measurement 4 (µm)	417.395	423.929	373.671	137.506	510.958	241.028	576.028	597.721	644.938	464.329
Measurement 5 (µm)	377.757	420.43	376.878	137.567	501.24	273.398	540.261	647.848	630.435	457.257
Average (µm)	313.80	436.27	372.79	144.12	502.52	248.22	570.31	622.96	652.91	455.04
Std Dev (µm)	157.97	15.61	6.11	14.43	10.00	39.09	22.46	21.79	17.97	15.41

THIS PAGE INTENTIONALLY LEFT BLANK

APPENDIX B. TRIAL'S ADHESION STRENGTH READINGS

The following table summarized the adhesion strength (MPa) readings from trials using 500 ºC and 1.38 MPa.

Spray Conditions / S/N	(a)	(b)	(c)	(d)	(e)
1	35.00	23.84	29.85	26.14	17.01
2	33.41	34.71	33.63	28.97	27.65
3	35.74	31.62	27.32	18	
4	42.02				
5	29.85				
6	37.22				
Average	35.54	30.06	30.27	24.37	22.33
Std Dev	3.70	4.57	2.59	4.65	5.32
Observations	Mixture of adhesive and coating failure	Mixture of adhesive and coating failure	Adhesion failure possibly due to thin coating formed by higher travel speed	Mixture of adhesive and coating failure	Mixture of adhesive and coating failure

THIS PAGE INTENTIONALLY LEFT BLANK

APPENDIX C. ACTUAL EXPERIMENT'S COATING THICKNESS MEASUREMENTS

Unit of Measurement: µm		Single Pass	Coated (Double Passes)	Annealed Coated
Zone 1	Measurement 1	173.913	435.729	457.199
	Measurement 2	105.135	442.872	446.486
	Measurement 3	152.217	414.301	428.705
	Measurement 4	148.551	421.444	457.199
	Measurement 5	148.551	428.571	428.586
Zone 2	Measurement 6	139.581	425.665	471.429
	Measurement 7	136.004	422.045	453.698
	Measurement 8	125.223	436.17	464.341
	Measurement 9	135.957	439.716	450.227
	Measurement 10	143.157	457.447	478.625
	Average	140.829	432.396	453.650
	Std Dev	17.074	11.961	15.469

THIS PAGE INTENTIONALLY LEFT BLANK

APPENDIX D. ACTUAL EXPERIMENT'S ADHESION TEST RESULTS

The following table summarized the specimens' adhesion strength measurements.

		Adhesion Strength (MPa)	Average (MPa)	Std. Dev.	Observations
Coated	**Measurement 1**	14.176	17.944	2.798	Coating failed
	Measurement 2	16.582			
	Measurement 3	20.126			
	Measurement 4	16.775			
	Measurement 5	22.063			
Annealed Coated	**Measurement 1**	45.892	46.564	0.672	Masterbond failed
	Measurement 2	47.236			

The following table show the thickness comparison between single pass and remnant of the 1st pass coatings. The coating remnant is slightly thicker than the single pass coating.

Unit of Measurement: µm		Single Pass	Remnant
Zone 1	**Measurement 1**	173.913	168.199
	Measurement 2	105.135	164.906
	Measurement 3	152.217	164.635
	Measurement 4	148.551	175.328
	Measurement 5	148.551	150.382
Zone 2	**Measurement 6**	139.581	
	Measurement 7	136.004	
	Measurement 8	125.223	
	Measurement 9	135.957	
	Measurement 10	143.157	
	Average	140.829	164.690
	Std Dev	17.074	8.127

THIS PAGE INTENTIONALLY LEFT BLANK

APPENDIX E. ACTUAL EXPERIMENT'S TENSILE TEST RESULTS

The following table shows the indicative load measurements when the coatings ruptured. Annealed coating's failure is more gradual without pronounced disruption to the load-displacement response. Hence, it is difficult to define the coatings' rupture load measurements.

Specimen Groups		Tensile 1	Tensile 2	Tensile 3	Tensile 4	Tensile 5	Tensile 6	Average	Std Dev
Rupture Load (N)	Coated	6426.112	6329.218	6678.299	6323.422	6375.634	6363.167	6415.975	122.083
	Annealed Coated	12484.9	Undefined	11426.02	Undefined	Undefined		11955.5	529.451

The following table summarized the respective specimens' final rupture displacement, ductility estimation, and the maximum load sustained.

Specimen Groups		Tensile 1	Tensile 2	Tensile 3	Tensile 4	Tensile 5	Tensile 6	Average	Std Dev
Substrate	Rupture Displacement (mm)	20.85498	20.21522	20.03718	20.3717	20.409		20.378	0.27246
	Ductility (%)	65.04984	63.05434	62.499	63.5424	63.6589		63.561	0.84984
	Max. Sustained Load (N)	10747.65	10665.67	10660.5	10499.8	10695.6		10653.838	83.0259
Annealed Substrate	Rupture Displacement (mm)	17.42618	16.90471	17.27249				17.201	0.21879
	Ductility (%)	54.3549	52.72835	53.87551				53.653	0.68243
	Max. Sustained Load (N)	11783.52	11927.38	12110.04				11940.312	133.614
Coated	Rupture Displacement (mm)	19.42743	19.48044	20.16187	20.1613	19.8858	19.8192	19.823	0.29071
	Ductility (%)	60.5971	60.76245	62.88793	62.8862	62.0269	61.8191	61.830	0.90678
	Max. Sustained Load (N)	11520.42	11618.91	11656.93	11555.9	11781.1	11562.9	11616.038	86.142
Annealed Coated	Rupture Displacement (mm)	15.87726	16.40331	16.18413	16.1567	15.7739		16.079	0.22629
	Ductility (%)	49.52358	51.16441	50.48075	50.3951	49.2012		50.153	0.70583
	Max. Sustained Load (N)	13500.03	13306.84	13375.74	13102.9	13036.3		13264.356	171.949

THIS PAGE INTENTIONALLY LEFT BLANK

APPENDIX F. ACTUAL EXPERIMENT'S NANOINDENTATION TEST RESULTS

	Substrate	Annealed Substrate	Coating	Annealed Coating
Max Displacement (nm)	1095.980	1048.046	815.182	977.551
Unloaded Displacement (nm)	989.061	932.192	661.136	871.221
Plasticity %	90.244	88.946	81.103	89.123
Successful Indentations	30	28	28	27
Average Young's Modulus (GPa)	104.264	132.056	120.697	134.292
Standard Deviation (GPa)	5.998	6.823	11.279	9.268
Average Hardness (GPa)	1.737	1.898	3.322	2.244
Standard Deviation (GPa)	0.328	0.161	0.48	0.253

THIS PAGE INTENTIONALLY LEFT BLANK

LIST OF REFERENCES

[1] Y. Li and C. Ning, "Latest research progress of marine microbiological corrosion and bio-fouling, and new approaches of marine anti-corrosion and anti-fouling," *Bioactive Materials,* vol. 4, p. 189–195, 2019.

[2] S. Yuan, A. M. Choong and S. Pehkonen, "The influence of the marine aerobic pseudomonas strain on the corrosion of 70/30 Cu–Ni alloy," *Corrosion Science,* vol. 49, p. 4352–4385, 2007.

[3] H. Koivuluoto, A. Milanti, G. Bolelli, L. Lusvarghi and P. Vuoristo, "High-pressure cold-sprayed Ni and Ni-Cu coatings: Improved structures and corrosion properties," *Journal of Thermal Spray Technology ,* vol. 23, p. 98-103, January 2014.

[4] R. C. Rice, J. L. Jackson, J. Bakuckas and S. Thompson, "DOT/FAA/AR-MMPDS-01 Metallic Materials Properties Development and Standardization (MMPDS)," National Technical Information Service, Springfield, 2003.

[5] W. D. Callister, Jr and D. G. Rethwisch, Materials Science and Engineering : An Introduction, Hoboken: John Wiley & Sons, Inc., 2009.

[6] S. Pathak and G. C. Saha, "Development of Sustainable Cold Spray Coatings and 3D Additive Manufacturing Components for Repair/Manufacturing Applications: A Critical Review," *Coatings,* vol. 7, no. 122, pp. 1–27, 2017.

[7] S. Yin, X. Suo, Y. Xie, W. Li, R. Lupoi and H. Liao, "Effect of substrate temperature on interfacial bonding for cold spray of Ni onto Cu," *Journal of Materials Science ,* vol. 50, p. 7448–7457, 2015.

[8] Y. Xie, S. Yin, J. Cizek, J. Cupera, E. Guo and R. Lupoi, "Formation mechanism and microstructure characterization of nickelaluminum intertwining interface in cold spray," *Surface & Coatings Technology,* vol. 337, p. 447–452, 2018.

[9] A. Nastic, D. MacDonald and B. Jodoin, "The influence of feedstock powder," in *Cold Spray in the Realm of Additive Manufacturing, Materials Forming, Machining and Tribology*, Cham, Switzerland, Springer, 2020, pp. 33–85.

[10] J. Yang, J. Yang, J. Xie, Q. Wang and K. Qu, "Improved fatigue crack propagation performance of Q355B steel with cold sprayed A5052 and Al coatings," *Surface & Coatings Technology ,* vol. 378, 2019.

[11] P. Cavaliere, A. Silvello, N. Cinca , H. Canales, S. Dosta, I. G. Cano and J. Guilemany, “Microstructural and fatigue behavior of cold sprayed Ni-based superalloys coatings,” *Surface & Coatings Technology ,* vol. 324, p. 390–402, 2017.

[12] Y. Xiong and M.-X. Zhang, “The effect of cold sprayed coatings on the mechanical properties ofAZ91D magnesium alloys,” *Surface & Coatings Technology ,* vol. 253, p. 89-95, 2014.

[13] W. Sun, A. W. Y. Tan, N. W. Khun, I. Marinescu and E. Liu, “Effect of substrate surface condition on fatigue behavior of cold sprayed Ti6Al4V coatings,” *Surface & Coatings Technology ,* vol. 320, p. 452–457, 2017.

[14] C. Ziemian, M. Sharma, B. Bouffard, T. Nissley and T. Eden, “Effect of substrate surface roughening and cold spray coating on the fatigue life of AA2024 specimens,” *Materials and Design ,* vol. 54, p. 212–221, 2014.

[15] R. Ghelichi, S. Bagherifard, D. Mac Donald, M. Brochu, H. Jahed, B. Jodoin and M. Guagliano, “Fatigue strength of Al alloy cold sprayed with nanocrystalline powders,” *International Journal of Fatigue ,* vol. 65, p. 51-57, 2014.

[16] P. Cavaliere and A. Silvello, “Processing conditions affecting residual stresses and fatigue properties of cold spray deposits,” *International Journal of Advanced Manufacturing Technology ,* vol. 81, p. 1857–1862, 2015.

[17] P. Cavaliere and A. Silvello, “Fatigue behaviour of cold sprayed metals and alloys: critical review,” *Surface Engineering ,* vol. 32, no. 9, pp. 631–640, 2016.

[18] Y. Xie, M.-P. Planche, R. Raoelison, P. Hervé, X. Suo, P. He and H. Liao, “Investigation on the influence of particle preheating temperature on bonding of cold-sprayed nickel coatings,” *Surface & Coatings Technology ,* vol. 318, p. 99-105, 2017.

[19] T. Stoltenhoff, C. Borchers, F. Gartner and H. Kreye, “Microstructures and key properties of cold-sprayed and thermally sprayed copper coatings,” *Surface & Coatings Technology,* vol. 200, pp. 4947–4960, 2006.

[20] J. Barnes, V. Champagne, D. Ballard, T. J. Eden, B. Shoffner, J. K. Potter and D. E. Wolfe, “Mechanical and Microstructural Effects of Cold Spray Aluminum on Al 7075 using Kinetic Metallization and Cold Spray Processes,” Air Force Research Laboratory, Wright-Patterson Air Force Base, 2007.

[21] M. Sharma, T. Eden and B. Golesich, “Effect of Surface Preparation on the Microstructure, Adhesion, and Tensile Properties of Cold-Sprayed Aluminum Coatings on AA2024 Substrates,” *Journal of Thermal Spray Technology ,* vol. 24, p. 410–422, February 2014.

[22] A. Moridi, S. Hassani-Gangaraj, S. Vezzú, L. Trško and M. Guagliano, “Fatigue behavior of cold spray coatings: The effect of conventional and severe shot peening as pre-/post-treatment,” *Surface & Coatings Technology ,* vol. 283, p. 247–254, 2015.

[23] H. Koivuluoto, J. Lagerbom and P. Vuoristo, “Microstructural studies of cold sprayed Copper, Nickel, and Nickel-30% Copper coatings,” *Journal of Thermal Spray Technology,* vol. 16, no. 4, pp. 488–497, 2007.

[24] T. Paul, P. Nautiyal, C. Zhang, B. Boesl and A. Agarwal, “Role of in-situ splat sintering on elastic and damping behavior of cold sprayed aluminum coatings,” *Scripta Materialia,* vol. 204, pp. 1–5, 2021.

[25] Y. Yamamoto, S. Uemura and M. Kajihara, “Observations on diffusion-induced recrystallization in binary Ni/Cu diffusion couples annealed at an intermediate temperature,” *Materials Science and Engineering,* vol. A312, pp. 176–181, 2001.

[26] X. Chen , H. Sun, D. Chen, L. Wang and Q. Liu, “On recrystallization texture and magnectic property of Cu-Ni alloys,” *Materials Characterization,* vol. 121, pp. 149–156, 2016.

[27] S. Kumar, B. R. Bodapati, G. Vinay, K. V. Kumar, N. M. Chavan, P. S. Babu and A. Jyothirmayi, “Estimation of inter-splat bonding and its effect on functional properties of cold sprayed coatings,” *Surface & Coatings Technology,* vol. 420, pp. 1–17, 2021.

[28] G. Bae, J.-i. Jang and C. Lee, “Correlation of particle impact conditions with bonding, nanocrystal formation and mechanical properties in kinetic sprayed nickel,” *Acta Materialia ,* vol. 60, p. 3524–3535, 2012.

[29] G. Bae, K. Kang, H. Na, J.-J. Kim and C. Lee, “Effect of particle size on the microstructure and properties of kinetic sprayed nickel coatings,” *Surface & Coatings Technology ,* vol. 204, p. 3326–3335, 2010.

[30] T. Schmidt, H. Assadi, F. Gartner, H. Richter, T. Stoltenhoff, H. Kreye and T. Klassen, “From particle acceleration to impact and bonding in cold spraying,” *Journal of Thermal Spray Technology,* Vols. 18 (5-6), pp. 794–808, 2009.

[31] P. Nautiyal, C. Zhang, B. Boesl and A. Agarwal, “Interfacial deformation and failure mechanisms at the single-splat length scale revealed in-situ by indentation of cold sprayed aluminum microparticles,” *Materials Science & Engineering A,* vol. 824, pp. 1–10, 2021.

[32] Y. Zou, W. Qin, E. Irissou, J.-G. Legoux, S. Yue and J. A. Szpunar, “Dynamic recrystallization in the particle/particle interfacial region of cold-sprayed nickel coating: Electron backscatter diffraction characterization,” *Scripta Materialia ,* vol. 61, p. 899–902, 2009.

[33] W. Li, C. Huang, M. Yu and H. Liao, “Investigation on mechanical property of annealed copper particles and cold sprayed copper coating by a micro-indentation testing,” *Materials and Design ,* vol. 46, p. 219–226, 2013.

[34] Y.-K. Wei, Y.-J. Li, Y. Zhang, X.-T. Luo and C.-J. Li, “Corrosion resistant nickel coating with strong adhesion on AZ31B magnesium alloy prepared by an in-situ shot-peening-assisted cold spray,” *Corrosion Science ,* vol. 138, p. 105–115, 2018.

[35] A. Silvello, P. Cavaliere, A. Rizzo, D. Valerini, S. D. Parras and I. G. Cano, “Fatigue bending behavior of cold-sprayed Nickel-based superalloy coatings,” *Journal of Thermal Spray Technology ,* vol. 28, p. 930–938, 2019.

[36] G. Sundararajan, N. M. Chavan and S. Kumar, “The elastic modulus of cold spray coatings: Influence of inter-splat boundary cracking,” *Journal of Thermal Spray Technology,* vol. 22, no. 8, pp. 1348–1357, 2013.

[37] S. Yin, X.-f. Wang, W.-y. Li and B.-p. Xu, “Numerical investigation on effects of interactions between particles on coating,” *Journal of Thermal Spray Technology,* vol. 18, no. 4, pp. 686–693, 2009.

[38] S. Bagherifard and M. Guagliano, “Fatigue performance of cold spray deposits: Coating, repair and additive manufacturing cases,” *International Journal of Fatigue ,* vol. 139, 2020.

[39] Praxair Surface Technologies Inc, “Powder Solution Catalog,” Praxair Surface Technologies Inc, 2014.

[40] Praxair Surface Technologies Inc, “CU-116 Safety Data Sheet,” Praxair Surface Technologies Inc, 2014.

[41] AZO Material, “Copper Nickel Alloy 90/10 - UNS C70600 - Cupronickel,” Azom.com, [Online]. Available: https://www.azom.com/article.aspx?ArticleID=6297.

[42] Aviva Metals, “C70600 Copper Nickel “90/10” - C706 Copper Nickel Alloys | Aviva Metals,” Aviva Metals, [Online]. Available: https://www.avivametals.com/products/c70600-copper-nickel-90-10.

[43] Centerline (Windsor) Limited, “Centerline Supersonic Spray Technology - SST PX Manual-Automatic Split Cabinet,” Centerline (Windsor) Limited, 2021. [Online]. Available: https://www.supersonicspray.com/products/ssttm-px-manual-automatic-split-cabinet.

[44] Centerline (Windsor) Limited, “Centerline Supersonic Spray Technology - SST X-Feeder,” Centerline (Windsor) Limited, 2021. [Online]. Available: https://www.supersonicspray.com/products/SST%E2%84%A2%20X-Feeder.

[45] MTI Corporation, “1200 degree Celcius dual zone split tube furnance with optional quartz tube (60, 80, 100mm) & vacuum flanges - OTF-1200X-II-UL,” MTI Corporation, 2020. [Online]. Available: https://www.mtixtl.com/DualZoneSplitTubeFurnace-OTF-1200X-II-UL.aspx.

[46] Masterbond, “EP15ND-2 Product Information,” Masterbond.com, 2021. [Online]. Available: https://www.masterbond.com/tds/ep15nd-2.

[47] J-B Weld, “J-B Weld Twin Tube,” J-B Weld, 2021. [Online]. Available: https://www.jbweld.com/product/j-b-weld-twin-tube.

[48] Elcometer, “Elcometer 510 Automatic Pull-Off Adhesion Gauge,” Elcometer , 2021. [Online]. Available: https://www.elcometer.com/en/coating-inspection/adhesion-testers/pull-off-adhesion-testing/elcometer-510-automatic-pull-off-adhesion-gauge.html.

[49] Instron, “High Force Universal Testing Machines,” Instron, 2020. [Online]. Available: https://www.instron.com/en/products/testing-systems/universal-testing-systems/high-force-universal-testing-systems/-/media/literature-library/products/2020/08/high-force-universal-testing-machines.pdf?la=en&hash=17DE6B02D2345039B27847C67791CE14#page=22.

[50] Agilent Technologies, “Material testing and research solutions from Agilent: Polymers and rubber application compendium,” 2010. [Online]. Available: https://www.agilent.com/cs/library/applications/Materials_Polymers_Compendium.pdf.

[51] ASM Handbook Committee , Metals Handbook - Ninth Edition (Volume 9 - Metallography and Microstructures), Novelty: American Society for Metals, 1985.

[52] FEI, “Inspect F50| Manualzz,” FEI, 2014. [Online]. Available: https://manualzz.com/doc/41484555/inspect-f50.

[53] Nikon, “Epiphot-300-200,” Nikon, June 1999 . [Online]. Available: http://www.tehno.com/specification/epiphot-300-200.pdf.

INITIAL DISTRIBUTION LIST

1. Defense Technical Information Center
   Ft. Belvoir, Virginia

2. Dudley Knox Library
   Naval Postgraduate School
   Monterey, California